Zeitschrift: Schweizerische mineralogische und petrographische Mitteilungen = Bulletin suisse de minéralogie et pétrographie

Band: 56 (1976)

Heft: 2

Artikel: Mineral chemistry of eclogites and related rocks from the Voltri Group, Western Liguria, Italy

Autor: Ernst, W.G.

DOI: https://doi.org/10.5169/seals-43688

Nutzungsbedingungen

Die ETH-Bibliothek ist die Anbieterin der digitalisierten Zeitschriften auf E-Periodica. Sie besitzt keine Urheberrechte an den Zeitschriften und ist nicht verantwortlich für deren Inhalte. Die Rechte liegen in der Regel bei den Herausgebern beziehungsweise den externen Rechteinhabern. Das Veröffentlichen von Bildern in Print- und Online-Publikationen sowie auf Social Media-Kanälen oder Webseiten ist nur mit vorheriger Genehmigung der Rechteinhaber erlaubt. Mehr erfahren

Conditions d'utilisation

L'ETH Library est le fournisseur des revues numérisées. Elle ne détient aucun droit d'auteur sur les revues et n'est pas responsable de leur contenu. En règle générale, les droits sont détenus par les éditeurs ou les détenteurs de droits externes. La reproduction d'images dans des publications imprimées ou en ligne ainsi que sur des canaux de médias sociaux ou des sites web n'est autorisée qu'avec l'accord préalable des détenteurs des droits. En savoir plus

Terms of use

The ETH Library is the provider of the digitised journals. It does not own any copyrights to the journals and is not responsible for their content. The rights usually lie with the publishers or the external rights holders. Publishing images in print and online publications, as well as on social media channels or websites, is only permitted with the prior consent of the rights holders. Find out more

Download PDF: 23.01.2026

ETH-Bibliothek Zürich, E-Periodica, https://www.e-periodica.ch

Schweiz. mineral. petrogr. Mitt. 56, 293–343, 1976

Mineral Chemistry of Eclogites and Related Rocks from the Voltri Group, Western Liguria, Italy

By *W. G. Ernst* (Los Angeles)*)

With 21 figures and 10 tables

Abstract

Within the Beigua serpentinite, iron-rich metagabbroic lenses, some approaching 200 meters in thickness and 4 kilometers in length, have recrystallized in at least five recognizable stages. Mineral assemblages are: stages A and B = garnet + omphacite + rutile, representing pre- and post-mylonitization growth, respectively; stage C = glaucophane + garnet + rutile ± sphene ± barroisitic hornblende ± epidote-clinozoisite; stage D = barroisitic hornblende + albite + chlorite + epidote-clinozoisite + sphene; and stage E = aluminous actinolite + albite + chlorite + epidote-clinozoisite + sphene. Phengite or paragonite developed in some stage D or E rocks, rare biotite chiefly in stage D.

Garnets are systematically enriched in Fe and Mg, depleted in Ca and Mn proceeding from stage A cores to stage B (and C) rims. Post mylonitic stage B omphacites are Na- and Al-rich compared to the more diopsidic premylonitic stage A clinopyroxenes. Sodic amphiboles of stage C appear to be enriched in ferrous iron and aluminum (ferroglaucophanes) rather than being pseudobinary glaucophane-riebeckite solid solutions. Calcic amphiboles of stages C and D are strongly enriched in Na and in both Al^{IV} and Al^{VI} (barroisites) relative to the greenschistic aluminous actinolites of stage E. Analyzed epidote-clinozoisites are ferric iron-rich in stage D, Al-rich in stage E schists. Most of the chlorites are ripidolites, and the sodic plagioclases are virtually pure albites; neither phase exhibits obvious compositional variation with metamorphic grade.

Chemographic analysis demonstrates the high chemical variance of the investigated assemblages, and the relatively high-pressure, low μH_2O nature of the earlier mineralogic stages compared to the later amphibolitic and greenschistic assemblages.

Fractionation of iron and magnesium, and of Ti and Mn between coexisting pairs of mafic silicates reveals widespread non-attainment of chemical equilibrium, as indicated by scatter of the data in many cases. Some tentative conclusions may be drawn, however. Stage A omphacite + garnet pairs exhibit more or less systematic iron-magnesium distribution with $K_D \approx 30$. Glaucophane replaced preexisting omphacite, hence garnet rim + glaucophane partition values ($K_D \approx 28$) may reflect an inherited stage B garnet + clinopyroxene fractionation of Fe^{2+} and Mg. The partitioning of titanium between coexisting

*) Department of Geology, Institute of Geophysics and Planetary Physics, University of California, Los Angeles, California 90024. IGPP publication no. 1637.

phases is obscured because of post-crystallization exsolution during annealing. Omphacites and calcic amphiboles accepted large amounts of Ti at early stages but subsequently expelled this element. In contrast, glaucophane and chlorite rejected Ti during their growth. Garnet cores are rich in Ti relative to rim compositions, but exsolution was limited. Mn is enriched in garnet relative to chain silicates. Disproportionation of manganese between calcic amphiboles and chlorite was not marked.

Based on analogies with previously available phase equilibrium experiments, oxygen isotopic data for somewhat similar parageneses, thermochemical calculations, and experimental determination of the pressure and temperature coefficients for K_D, physical conditions attending the metamorphic recrystallization sequence developed in the Ligurian eclogitic rocks have been estimated. Stage A assemblages are deduced to have formed at $430 \pm 50°$ C and about 10 kilobars confining pressure, with stage B conditions including slightly higher temperatures and pressures. Garnet + glaucophane rocks of stage C are thought to have formed at approximately 400° C and 8 kilobars P_{total}, attended by increased values of μH_2O relative to the preceding stages. Strong depressurization and slight cooling is postulated to have characterized the passage of these rocks through stage D and E conditions, namely 300–375° C and 2–5 kilobars total pressure. The chemical potential of H_2O probably was high, as reflected by the hydrous nature of the assemblages; moreover, the presence of a separate aqueous phase is indicated by strong metasomatic effects displayed in the amphibolites and greenschists.

The regional geology and previous large-scale syntheses are compatible with the petrotectonic history proposed here, which involved southward and eastward subduction of a Tethyan lithospheric plate containing the Beigua serpentinite + included lenses of ferrogabbro, and concomitant, increasingly high-pressure metamorphism of stages A and B, interrupted by a period of deformation. A gradual introduction of aqueous fluid accompanied the apparent decoupling of the buoyant Beigua serpentinite + included eclogitic layers from the descending slab; the inception of uplift of the complex is reflected by growth of sodic amphibole during stage C. Subsequent relatively rapid (adiabatic) rise towards the surface is attested to by production of the successively more hydrous amphibolites and greenschists of stages D and E at slightly reduced temperatures and at much lower pressures.

GEOLOGIC AND TECTONIC SETTING

Metamorphism of the Alps during late Mesozoic and early Tertiary time involved a number of different stages, as has been well documented by numerous petrologists and geochronologists over the past 15–20 years (e.g., Van der Plas, 1959; Bearth, 1959, 1966, 1967, 1971; Niggli, 1960, 1970; Niggli and Niggli, 1965; Wenk, 1962, 1970; Wenk and Keller, 1969; Jäger et al., 1967; Hunziker, 1970, 1974; Frey et al., 1974; Miller, 1974). It is now generally considered that the early portion of this recrystallization accompanied the closure of Mesozoic Tethys, apparently through a geometrically complicated low-angle subduction along a southward and eastward (internally) dipping plate junction – or series of junctions – and the subsequent collision of the northern, more external European foreland and adjacent more southerly oceanic section

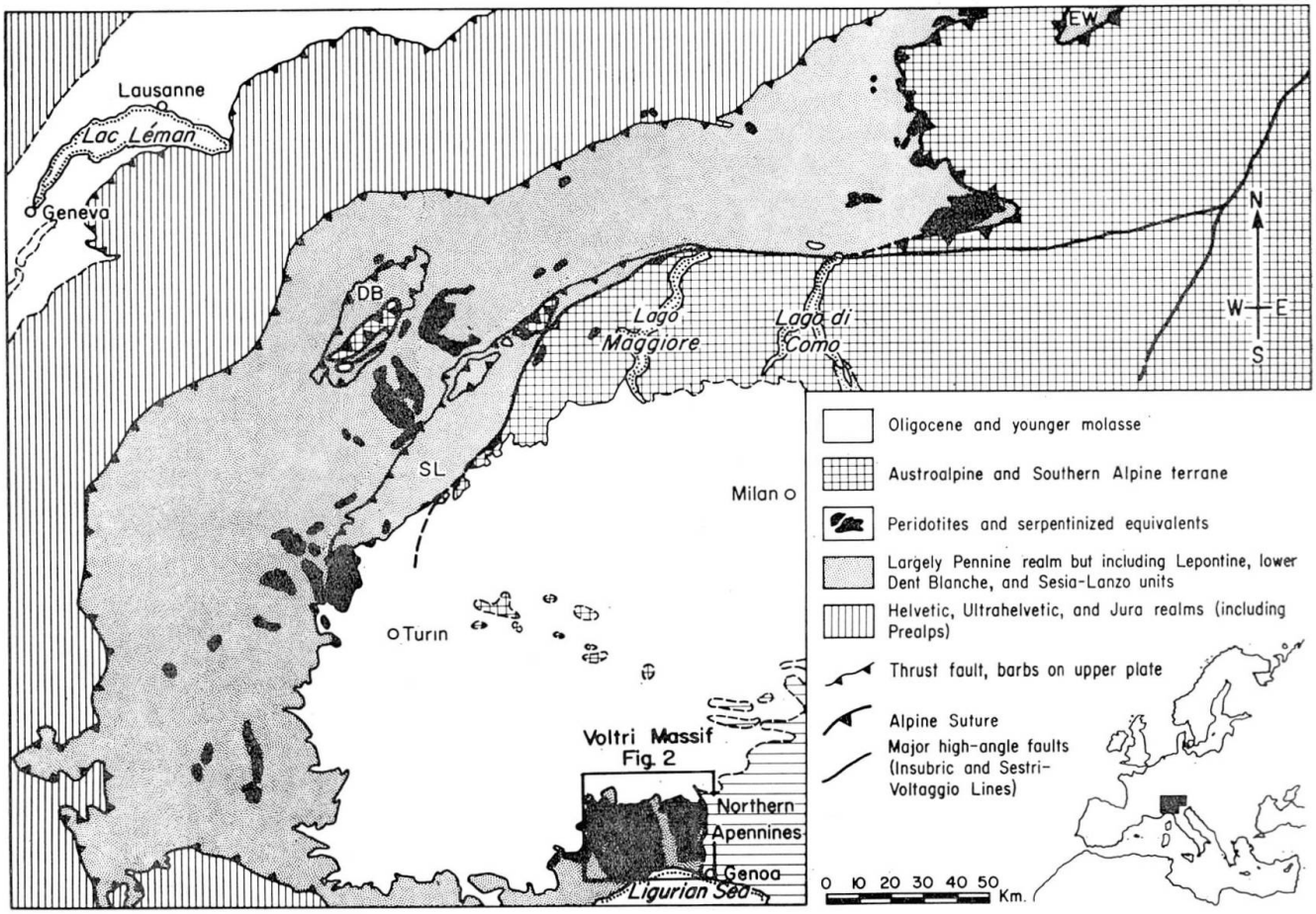

Fig. 1. Regional geology of the western Alps, simplified from the 1 : 1,000,000 scale metamorphic map of the Alps, general coordinator, E. Niggli (1973). Fold vergence is directed externally, that is, away from the Po molasse. The subhorizontal tectonic contact between the overlying South Alpine + Austraoalpine rocks of the Insubrian plate (Dal Piaz, 1974a, b) and the more external, subjacent Pennine, Helvetic, Sesia-Lanzo and Lepontine realms of the European-Tethyan plate is an imbricate zone termed the Alpine Suture and thought to represent the initial convergent plate margin (Ernst, 1971, 1973). Some, but not all, of the ultramafic bodies shown in the western Alps belong to the Insubrian plate, hence lie above this tectonic contact. Components of strike slip along the Insubric and Sestri-Voltaggio lines (Scholle, 1970; Laubscher, 1971a, b) have resulted in truncation and partial obliteration of the original plate boundary. The Engadine window is abbreviated EW.

with the internal, continental crust-capped lithospheric plate of the Southern Alps + Austroalpine terrane (Ernst, 1971, 1973; Dal Piaz et al., 1972; Dal Piaz, 1974a, b; Dewey et al., 1973). This convergence brought allochthonous slices of subducted ophiolite (Tethyan deep-sea sedimentary cover, oceanic crust and uppermost mantle) and detached segments of the non-subducted (obducted) mantle of the southern plate over the more northerly terrane. The regional geology of the western Alps is shown in greatly simplified form in Fig. 1.

The juxtaposed sections have been strongly imbricated and much modified by later deformation and recrystallization, but the effects of the early Alpine event are still evident in relatively high-pressure mineral assemblages preserved

especially well in the Franco-Italien Alps (BOCQUET, 1971; CHATTERJEE, 1971) and in southwestern Switzerland (BEARTH, 1970, 1973, 1974). Among the best known of these are the eclogitic and amphibolitic parageneses of the Zermatt–Saas Fee region (BEARTH, 1959, 1967; WETZEL, 1974) and the eclogitic mica schists and related rocks of the Sesia–Lanzo zone (VITERBO-BASSANI and BLACKBURN, 1968; DAL PIAZ et al., 1971; COMPAGNONI and MAFFEO, 1973). None of these occurrences is as spectacular, however, as the eclogitic layers which occur in the Voltri complex of the Ligurian Alps (BOCCHIO and MOTTANA, 1974; MOTTANA and BOCCHIO, 1975; CORTESOGNO et al., 1975 and in press). As can be seen from Fig. 1, this lherzolite and serpentinized peridotite is the largest body of its kind in the western (and eastern) Alps. Within it, eclogitic rocks are preserved on an unprecedented scale: some layers in the ultramafic host are as much as 4 km in length and more than 200 m in thickness. The general geologic relations are shown in Fig. 2.

The Gruppo di Voltri consists of three principal map units: (1) the Erro-Tobbio plagioclase lherzolites and serpentinized equivalents; (2) the Beigua serpentinite and included lenses and layers of eclogitic rocks; and (3) the "calcescisti" and related volcanosedimentary schists. Other lithologic units include the granitic Savona-type basement, which may be correlated with similar rocks of the European foreland and displays evidence of incipient high-pressure early (?) Alpine metamorphism (CORTESOGNO et al., in press), the ophiolite-bearing feebly recrystallized argillaceous and calcareous sedimentary rocks of the Northern Apennines (Eastern Liguria), and the late- to post-orogenic Oligocene and younger molasse of the Po Plain.

The Erro-Tobbio plagioclase lherzolites possess a tectonite fabric and are partially transformed to lizardite- and antigorite-bearing units. Included metagabbros to some extent have been converted to greenschist assemblages, but show no evidence of having passed through an eclogitic stage. Both mafic and ultramafic rocks carry abundant relics of the original mineral assemblages.

In contrast, the antigoritic Beigua serpentinite is thoroughly schistose, and the phase assemblage of the protolith has been totally obliterated. The mafic lenses, however, bear testament to a long and complex recrystallization history. Textures of the parental gabbros are well preserved in many of the metamorphic rocks, and a few eclogites contain relict igneous titanaugite. The eclogitic paragenesis of these layers will be described in the next section.

Schists of the Sestri-Voltaggio zone, and the "calcescisti" – the *schistes lustrés* of the Franco-Italian Alps – consist of micaceous, calcareous and siliceous schists with interlayered metamorphosed mafic units. Mineral assemblages are predominantly prasinitic (greenschistic with porphyroblastic albite) but relics of an earlier glaucophane schist stage are preserved sporadically. Locally, rare relics of Na pyroxene, garnet and/or rutile occur as pre-blueschistic phases.

The interleaved Beigua serpentinite and "calcescisti," which share both low-

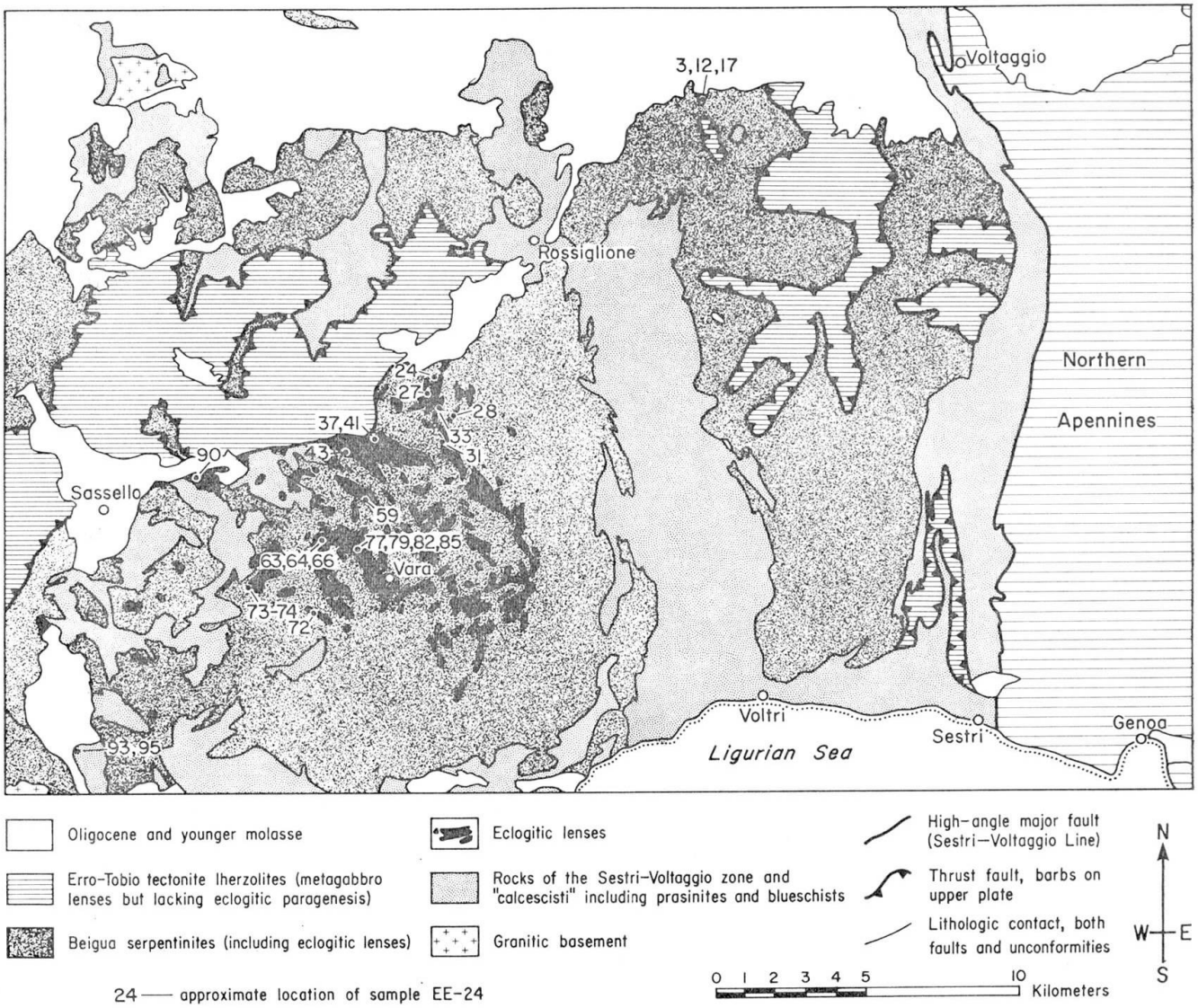

Fig. 2. Geology Western Liguria, with emphasis on the Gruppo di Voltri, simplified after Messiga and Piccardo (1974), Chiesa et al. (1975) and Cortesogno et al. (in press). The gabbros parental to the eclogitic rocks seem to have been intruded into the host Beigua ultramafic mass. The Oligocene and younger molasse rests unconformably on all map units. With these exceptions, all lithologic contacts shown are tectonic, the most profound of which is the low-angle thrust fault separating the Tobbio-Erro plagioclase lherzolite above from the rest of the Voltri complex below. This break is thought to represent a portion of the Alpine Suture. The approximate locations of 25 microprobed specimens (in all, 95 samples were studied petrographically by Cortesogno et al., in press) are also indicated; EE prefixes habe been omitted for clarity.

and high-angle faulted, convoluted contacts, have been tectonically emplaced over the structurally lower, essentially autochthonous sialic basement. All these rocks contain mineralogic evidence of relatively high-pressure metamorphism, but the lack of eclogitic parageneses in the "calcescisti," metamorphic rocks of the Sestri-Voltaggio zone and Savona-type granites, argues for a post-eclogitic stage juxtaposition of the Beigua serpentinite + eclogite against these other units. Overlying this complex along a subhorizontal thrust fault is the feebly

recrystallized Erro-Tobbio lherzolitic unit, which evidently was not affected by the high-pressure subduction event. CORTESOGNO et al. (in press) have suggested that the Erro-Tobbio peridotite represents a part of the leading edge of the southern or Insubrian plate (DAL PIAZ, 1974a, b) and that this low-angle thrust contact is a segment of the former convergent plate junction (the Alpine Suture of ERNST, 1973).

The Northern Apennines probably represent another portion of the non-subducted Insubrian lithospheric plate, which has been brought into contact with the Voltri complex along the high-angle Sestri-Voltaggio Line in response to the post-convergence counterclockwise rotation of Italy (ZIJDERVELD et al., 1970; LOWRIE and ALVAREZ, 1975; CHIESA et al., 1975).

PARAGENESIS OF THE ECLOGITIC ROCKS

Mineral assemblages of the eclogitic lenses within the Beigua serpentinite have been described by BOCCHIO and MOTTANA (1974) and by CORTESOGNO et al. (1975; in press). Modes of 95 rocks studied in the present investigation, and 83 new bulk-rock analyses, are described by CORTESOGNO et al. (in press) and the interested reader is referred to that paper for details. Sample locations are shown in Fig. 2. Although intergradations exist, five distinct metamorphic stages in the formation of phase assemblages can be recognized in the Voltri eclogitic rocks: earlier and later eclogitic stages (A and B, respectively), then glaucophanic, barroisitic and greenschist + prasinitic stages (C, D and E, respectively). The earlier, eclogitic, stages are best preserved within the central portions of the mafic layers whereas the effects of amphibolitization and prasinitization are better developed near the margins of the lenses in contact with serpentinite. Many outcrops show relics of all five stages in representative hand specimens. The mineral paragenesis is illustrated in Fig. 3, and summarized briefly below.

Stage A. This stage is characterized by the growth of large anhedra of omphacite and garnet, plus small scattered prisms of rutile. The igneous plagioclase and titanaugite are efficiently pseudomorphed, in part by a granular aggregate of Na-pyroxene in the former case, and by single porphyroblasts of Na-pyroxene in the latter. Both types of omphacite exhibit selvages of fine-grained garnet, or coagulated granoblastic clots.

Stage B. Ensuing cataclasis to some extent modified or obliterated the earlier pseudoigneous textures and resulted in the production of both compositional and grain-size layering. Many such eclogites, however, retain relict early pseudomorphic omphacite. Newly generated Na-pyroxene builds granular-to-pris-

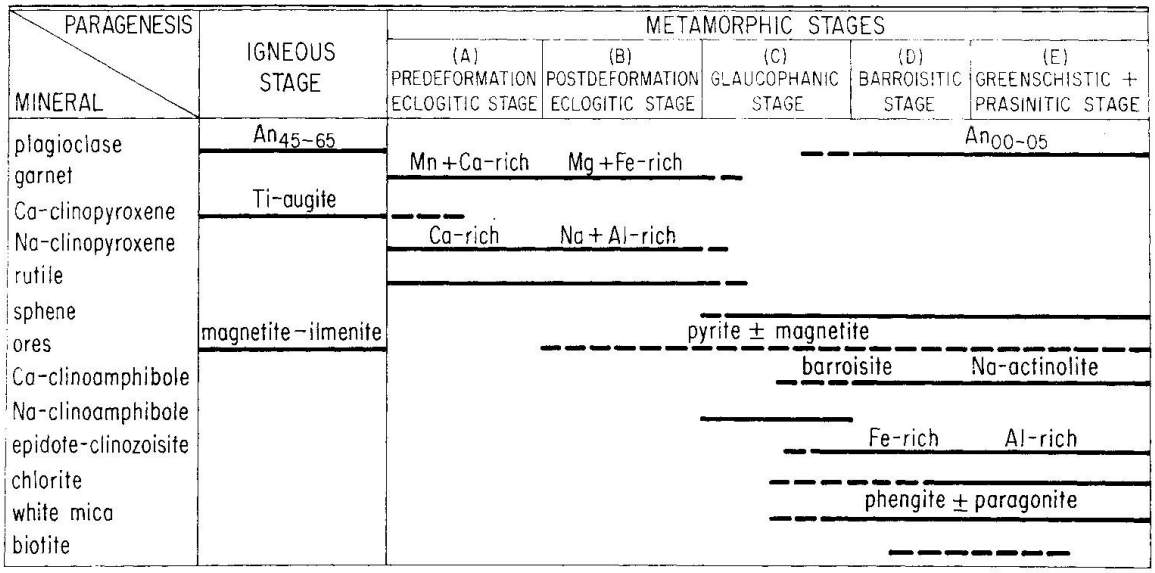

Fig. 3. Stages of mineral development and replacement in metagabbroic bodies enclosed within the Beigua serpentinite, Voltri Massif, largely after CORTESOGNO et al. (in press). A solid line indicates the presence of a phase in essentially all rocks of that stage, whereas a dashed line signifies irregular or sporadic occurrences. The assemblages shown reflect the persistance of metastable relics as well as equilibrium associations. The post-intrusion but preeclogitic conversion of some gabbroic layers to rodingitic compositions and assemblages is not illustrated. Major deformation took place chiefly between stages A and B, and approximately between stages C and D.

matic, moderately strongly oriented aggregates, whereas garnet occurs as large, somewhat rotated subhedra. Rutile is present as trains of very small grains parallel to the superimposed foliation. During this stage, much of the early clinopyroxene seems to have exsolved lamellae of a titanium oxide phase.

Stage C. The replacement of omphacite and garnet cores by prismatic glaucophane marks the commencement of stage C recrystallization. Rutile accompanies the blue amphibole, but locally it is armored and replaced by sphene. Some garnets probably continued to grow as indicated by their euhedral rims against Na-amphibole, but their cores were certainly unstable. The sequential appearance and coexistence with glaucophane of epidote and barroisite, and the ultimate reaction of rutile and of garnet rims provided transition to the next stage, more or less accompanied by deformation of the earlier textures.

Stage D. Here barroisitic amphibole (blue-green hornblende), armoring and replacing glaucophane, becomes the major phase. It is accompanied by interstitial albite, an epidote mineral, sphene and diverse but sporadically developed layer silicates.

Stage E. This stage is characterized by the exsolution of an iron-titanium oxide phase from the early Ca clinoamphibole, by the replacement of barroisitic hornblende by actinolite and by the porphyroblastic enlargement of albite. Biotite is obliterated as greenschistic assemblages pervasively replace earlier phase compatibilities.

COMPOSITION OF MINERALS

Techniques employed

All phases were analyzed employing an ARL SEMQ microprobe situated in the Institut für Kristallographie und Petrographie, Eidgenössische Technische Hochschule, Zürich. This particular instrument possesses two semiscanners and four programmed drive scanners. Analytical conditions were: accelerating voltage 15 kv; specimen current 50 nannoamps; and spot size about one-half to one micron. The semiscanners were adjusted for SiK_α and AlK_α radiation with predetermined values of background employed for data reduction. Each of the four adjustable scanners was programmed using a PDP-11 on-line computer to measure low 2θ background (10 seconds), preset peak intensity (20 seconds), and high 2θ background (10 seconds), for each of two elements; the four channels provided values for Mg, Fe, Ca, Ti, Na, K, Mn and Cr. Between two and five 20 second counts for different analytical locations were averaged after a first approximation comparison with a compositionally similar set of seven or eight mineral reference standards. The averaged data, corrected for drift, background and dead time, were reduced using the on-line computer employing Bence-Albee methods, and the output presented in terms of oxide weight percents by means of a teletypewriter.

Samples of 25 rocks were selected after petrographic examination of 95 specimens (CORTESOGNO et al., in press) for their apparent phase homogeneity. Polished thin sections were prepared, studied once more petrographically, and carbon coated. In spite of attempts to avoid the problem, compositional zoning was detected in some phases, especially garnets, and in a few epidote group minerals and calcic amphiboles. Where significant zoning was found, analytical data are presented for core and/or rim compositions and are so indicated in the tables. In cases where alkali or hydroxyl devolitilization during beam impingence was encountered, the sample was moved slightly during the analysis to prevent heating, but only analyses for specimens which retained constancy of counting rate are presented in the tables.

Approximate H_2O contents for OH-bearing phases were assumed for purposes of the Bence-Albee data reduction, and for presentation in the tables, but these values need not be entirely correct. However, they have been chosen so as to be comparable with those generally indicated in published gravimetric analyses. Weight percent H_2O values selected were as follows: amphiboles and epidote group minerals, 2.0; micas, 4.0; and chlorite, 12.0.

Ferric-ferrous ratios cannot be unambiguously obtained by electron microprobe analysis, although several logical schemes for deducing them from the machine output have been devised. The author looks with some misgivings on such computations where complicated phases such as amphiboles and micas are involved because the numerous chemical substitutions and analytical uncertainties allow a multiplicity of methods of obtaining charge balance and reasonable cation proportions. Moreover, the computational approach has the psychological effect of assuring the unwary reader that the stated composition is better known than, in fact, it actually is. Instead, the author has adopted a strictly pragmatic approach, and one which provides compositions closely similar to conventional "wet" analyses of analogous minerals. For sodic plagioclases and epidotes, all iron is calculated as ferric. In contrast, the iron is cast as ferrous in one relict igneous augite and in all garnets, calcic amphiboles, layer silicates and sphene. In the case of sodic pyroxenes and sodic amphiboles, where the molecular proportion of Na exceeds Al, one half the iron is somewhat arbitrarily figured as Fe^{3+}, the other half as Fe^{2+}.

Analytical data are presented for 21 garnets, 18 clinopyroxenes, 10 sodic amphiboles,

21 calcic amphiboles, 16 epidote group minerals, 13 chlorites, 13 sodic plagioclases, 7 micas and 3 sphenes in Tables 1–9, respectively. Cation properties were calculated on an anhydrous basis for all analyzed minerals assuming, where required, the stoichiometrically ideal hydroxyl contents. In the interest of saving space, these cation proportions are not presented in the tables, but they were utilized to eliminate crystallochemically implausible analyses. An indication of the accuracy of the tabulated data may be obtained by examining the oxide totals and their deviations from an ideal 100 percent. Moderate deviations are expected due to the required approximations regarding volatile contents and ferrous-ferric ratios previously discussed, as well as the limited number of elements analyzed for.

Garnets

The 21 garnet analyses listed in Table 1 exhibit remarkably little chemical variation. For six samples, compositions of both interiors and peripheries of the grains have been determined. In general, cores may be correlated with stage A growth, rims with stage B (and minor C) enlargement. None of the samples carry any potash, chrome is negligible, and soda and titania contents average 0.02 and 0.08 weight percents, respectively. There is a faint tendency for the

Table 1. *Electron microprobe analyses of garnets from eclogitic rocks, Gruppo di Voltri, Ligurian Alps*

	Sample number									
Oxide	EE-3 core	EE-3 rim	EE-31	EE-37 rim	EE-43 rim	EE-59 rim	EE-63 rim	EE-64 core	EE-64 rim	EE-66 rim	EE-72 core
SiO_2	37.26	37.24	37.20	36.88	36.97	36.69	37.33	36.49	36.71	36.64	35.83
Al_2O_3	20.45	20.46	20.42	20.13	21.15	21.12	21.63	20.59	21.09	21.03	21.51
TiO_2	0.05	0.07	0.14	0.06	0.06	0.10	0.05	0.05	0.02	0.08	0.21
FeO	33.45	33.74	31.42	34.91	33.33	32.43	30.85	29.15	34.91	35.34	33.19
Cr_2O_3	0.00	0.01	0.00	0.00	0.00	0.00	0.00	0.00	0.00	0.00	0.00
MgO	1.65	2.38	1.75	2.35	1.86	1.09	3.98	0.35	1.70	1.28	1.39
MnO	1.51	0.30	2.03	0.78	0.71	1.19	0.05	3.88	0.43	0.42	1.98
CaO	4.92	5.12	6.25	2.72	5.27	6.57	5.05	8.06	3.66	4.32	5.09
Na_2O	0.03	0.00	0.02	0.02	0.00	0.00	0.00	0.00	0.03	0.02	0.05
K_2O	0.00	0.00	0.00	0.00	0.00	0.00	0.00	0.00	0.00	0.00	0.00
Total	99.32	99.32	99.23	97.85	99.36	99.18	98.94	98.57	98.55	99.13	99.25

	Sample number									
Oxide	EE-77 core	EE-77 rim	EE-79 core	EE-79 rim	EE-82 core	EE-82 rim	EE-85 core	EE-85 rim	EE-93 core	EE-95 core
SiO_2	36.91	36.55	36.85	36.81	37.29	37.16	35.20	34.84	36.28	35.99
Al_2O_3	21.51	21.58	21.39	21.67	21.41	21.83	21.22	21.59	21.53	21.55
TiO_2	0.20	0.00	0.15	0.02	0.13	0.00	0.14	0.08	0.08	0.10
FeO	29.94	35.80	33.04	35.26	31.50	34.48	32.53	35.69	29.46	31.32
Cr_2O_3	0.00	0.00	0.00	0.00	0.00	0.00	0.00	0.00	0.04	0.04
MgO	0.64	1.65	1.12	1.50	1.41	2.02	1.42	1.41	1.58	1.43
MnO	1.72	0.84	1.18	0.87	1.97	0.61	1.56	0.26	9.27	7.94
CaO	9.34	3.24	6.32	4.03	7.43	4.39	5.72	4.60	2.32	1.84
Na_2O	0.00	0.01	0.02	0.02	0.01	0.07	0.01	0.01	0.02	0.02
K_2O	0.00	0.00	0.00	0.00	0.00	0.00	0.00	0.00	0.00	0.00
Total	100.25	99.68	100.09	100.18	101.15	100.56	97.78	98.48	100.59	100.23

cores to be enriched in Ti relative to the margins. The extreme values for silica and alumina contents are 34.84–37.33 and 20.13–22.14 weight percents, respectively. The most important chemical variations in garnets involve the differences between core and rim compositions in terms of CaO, MgO, MnO and FeO; even so, the percentage variation of the last mentioned oxide (range 29.15–

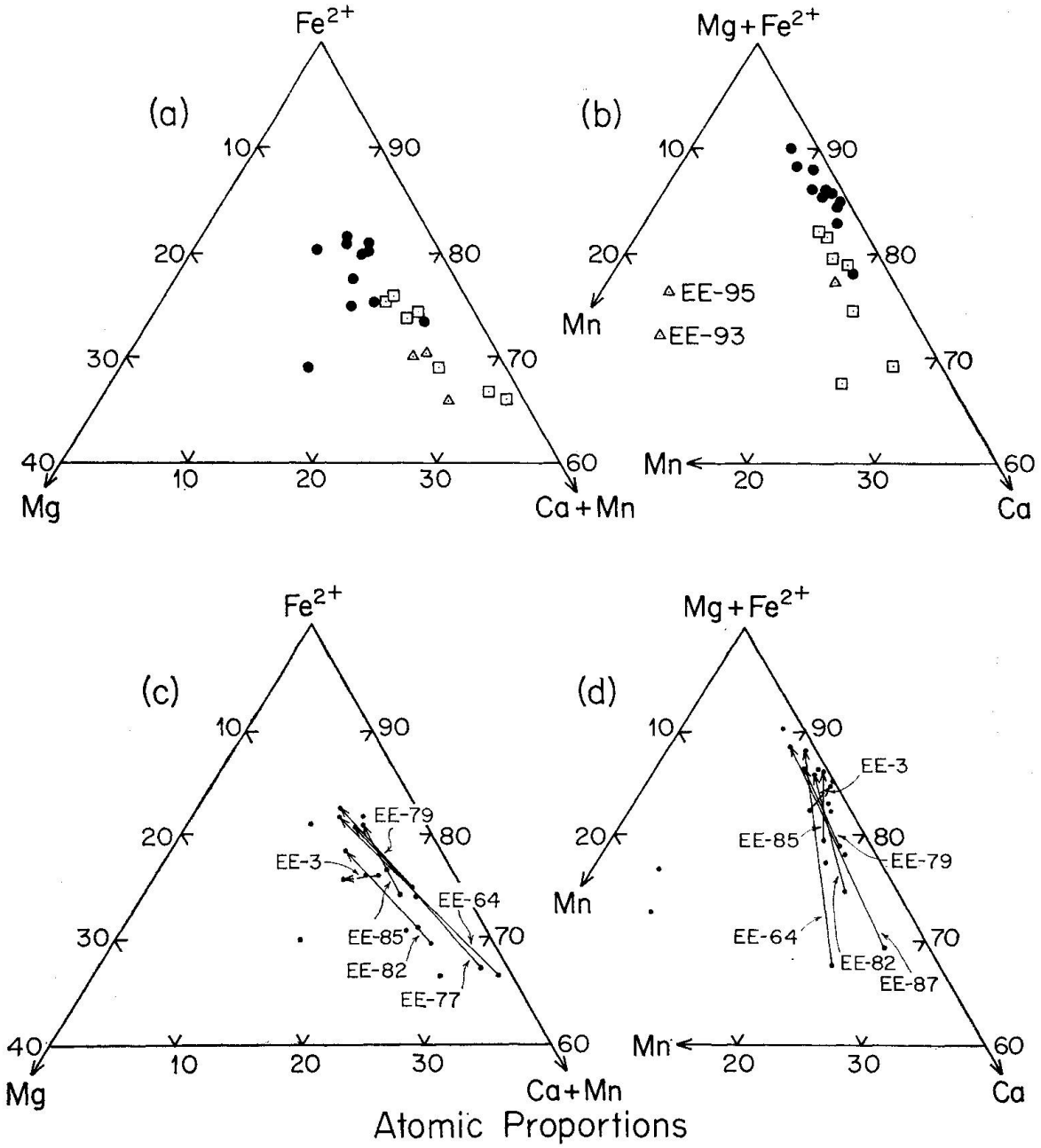

Fig. 4. Ternary atomic proportions of Alm-Py-Gross + Spess (a, c) and of Alm + Py-Spess-Gross (b, d) for garnets from the Voltri eclogitic rocks. Note that only the iron-rich apexes of the diagrams are shown. In (a) and (b), filled circles signify rim compositions, open squares and triangles designate cores and homogeneous grains, respectively. In (c) and (d), dots indicate garnet analyses, arrows point to rim values for six pairs of core-rim analytical data.

35.80) is rather small. Based on 12 oxygens, eight of the 21 analyses exhibit slight deficiencies of Al (+Ti) required to fill both octahedrally coordinated positions, necessitating a maximum of only 0.044 Fe^{3+} per formula unit to maintain the ideal stoichiometry. The negligible amount of ferric iron required on crystallochemical grounds supports the assumption that essentially all of the Fe is divalent in these garnets. Therefore, we are justified in regarding the Voltri garnets as quaternary solid solutions in the system Alm-Py-Spess-Gross, the proportions of And and Uvar having been shown to be inconsequential. In Fig. 4, the Fe^{2+}/Mg/Ca/Mn ratios for the analyses are presented; this illustration basically shows the proportions of metal atoms accupying the large eightfold coordinated site in garnet.

As is clear from Fig. 4, these garnets are essentially calcium-, magnesium- and manganese-bearing almandines, the proportion of the $Fe_3^{2+}Al_2Si_3O_{12}$ end member ranging from 66.0 to 81.8 mole percent. Figs. 4a and b demonstrate that there is a tight clustering of garnet rim compositions near the value $Alm_{78}Py_{08}Gross_{12}Spess_{02}$. Core chemistries are more difficult to adequately sample, but compositions in the central portions of the garnets tend to be enriched in Ca and Mn at the expense of iron and magnesium. Six core + rim zonal sequences are illustrated in Fig. 4c and d. With the exception of the measured zoning of sample EE-3, they show a systematic increment in $Mg + Fe^{2+}$ towards the grain margins. A difficulty in measuring the zoning results from the partial replacement of the peripheries of some relict garnets by later assemblages – hence the analyses of anhedral garnets, as is commonly the case in the Voltri eclogitic rocks, does not necessarily provide the compositions of the true rims. Finally, it should be noted that traces of anhedral garnet preserved in prasinites EE-93 and EE-95 are exceptionally manganese-rich, containing 21.0 and 18.2 mole percents Spess end member, respectively (Fig. 4b); most probably these represent metastable relict cores which have persisted from an earlier eclogitic stage, inasmuch as CORTESOGNO et al. (in press) report only 0.22 and 0.19 weight percents MnO in the parent rocks.

Clinopyroxenes

Analyses of 18 clinopyroxenes are listed in Table 2. Of these, one is a relict igneous augite, seven represent premylonitization omphacite (stage A) and the remaining ten crystallized after the first deformation (stage B). Of the latter, two (EE-3 and EE-3′) are replicate analyses for different parts of the microprobe section and provide an indication of the phase homogeneity.

The pre-eclogitic stage gabbroic clinopyroxene differs from the metamorphic clinopyroxenes in that it contains 0.48 weight percent TiO_2 versus an average of 0.09 weight percent titania for the 17 analyzed omphacites. Alumina (2.01),

Table 2. *Electron microprobe analyses of clinopyroxenes from eclogitic rocks, Gruppo di Voltri, Ligurian Alps*

	Sample number								
Oxide	EE-3 B	EE-3′ B	EE-17 A	EE-28 augite	EE-31 A	EE-43 A	EE-43 B	EE-63 A	EE-64 B
SiO_2	55.61	55.21	56.05	50.77	54.96	55.86	55.91	55.10	54.84
Al_2O_3	7.44	7.86	8.31	2.01	5.98	7.78	9.32	5.82	8.31
TiO_2	0.06	0.05	0.15	0.48	0.06	0.09	0.05	0.04	0.08
Fe_2O_3	7.91	7.00	1.52	–	5.26	5.52	6.45	4.65	6.25
FeO	7.12	6.31	1.37	8.06	4.74	4.98	5.80	4.19	5.62
Cr_2O_3	0.00	0.00	0.83	0.02	0.00	0.00	0.00	0.00	0.00
MgO	4.62	5.07	10.45	11.64	7.98	6.37	4.19	8.61	5.46
MnO	0.00	0.04	0.03	0.26	0.03	0.00	0.14	0.00	0.02
CaO	8.24	9.42	15.63	20.99	13.69	11.84	7.35	14.18	11.08
Na_2O	10.04	9.37	5.66	0.79	6.35	7.42	10.60	6.57	8.17
K_2O	0.00	0.00	0.01	0.00	0.00	0.00	0.00	0.00	0.00
Total	101.04	100.33	100.01	95.02	99.05	99.86	99.81	99.16	99.83

	Sample number								
Oxide	EE-66 B	EE-72 A	EE-72 B	EE-77 B	EE-79 A	EE-79 B	EE-82 B	EE-85 A	EE-85 B
SiO_2	55.26	55.84	55.66	53.60	55.24	56.51	55.84	54.43	55.16
Al_2O_3	8.22	8.31	9.37	8.89	6.07	8.13	8.62	5.80	8.93
TiO_2	0.10	0.17	0.12	0.12	0.05	0.07	0.09	0.17	0.09
Fe_2O_3	6.00	4.73	6.74	5.26	6.83	6.12	5.62	7.07	5.31
FeO	5.40	4.27	6.08	4.73	6.16	5.52	5.06	6.36	4.77
Cr_2O_3	0.00	0.00	0.04	0.00	0.00	0.00	0.00	0.00	0.00
MgO	5.96	7.72	4.55	6.60	7.08	6.66	6.63	6.68	6.56
MnO	0.01	0.05	0.19	0.00	0.00	0.03	0.04	0.03	0.00
CaO	11.22	12.11	10.70	12.04	13.60	11.70	11.78	12.91	11.71
Na_2O	8.01	7.12	8.05	7.43	6.66	7.69	7.69	6.64	7.55
K_2O	0.00	0.00	0.00	0.00	0.00	0.00	0.00	0.01	0.00
Total	100.09	100.32	101.50	98.67	101.69	102.43	101.37	100.10	100.08

silica (50.77) and soda (0.79) oxide contents are much lower, whereas MgO (11.64) and CaO (20.99) are distinctly higher than in the sodic clinopyroxenes. A few specimens contain measurable amounts of chrome, and EE-17 is exceptionally rich in Cr_2O_3 (0.83 weight percent); none of the analyzed clinopyroxenes carry essential potash. Small concentrations of manganese occur in most samples, but its distribution is quite irregular and does not seem to be systematic. The silica contents of the 17 eclogitic clinopyroxenes are remarkably constant, ranging only between the values 53.60 and 56.51. Thus the major compositional variations seem to be restricted to the elements Al, Fe, Mg, Ca and Na.

Except for the relict augite, the atomic proportions of sodium exceed those of octahedrally coordinated aluminum by roughly 40–100 percent, to some extent justifying the assumption employed here in regarding half of the iron as trivalent. The 10 analyzed stage B omphacites typically contain more total iron and all are less magnesian than the 7 premylonitization stage A sodic clinopyroxenes; two coexisting – but of course not equilibrium pairs – of A + B omphacites, EE-43 and EE-72, display a marked increase in the Fe_{total}/Mg ratio

passing from stage A to stage B crystallization, whereas for two other A + B pairs, EE-79 and EE-89, a modest decrease in Fe_{total}/Mg seems to have occurred. This difficulty in recognizing systematic compositional variation in iron is doubtless a consequence of the arbitrary constraint requiring the ferrous-ferric ratios to be treated as unity.

Figure 5 is a plot of Na + Ca per six oxygens for the metamorphic clinopyroxenes. Basically this diagram shows the occupancy of the large 6–8-fold structural site, M_2, in clinopyroxene. All 17 analyses lie very close to the dashed line marking pyroxene compositions which satisfy the constraint $\sum Ca + Na = 1.00$. Thus the Voltri omphacites exhibit insignificant solid solution towards En and/or Fs. Perhaps more importantly, there is an obvious compositional contrast between pre- and post-mylonitic omphacites, with the stage B clinopyroxenes consistently enriched in Na relative to the stage A clinopyroxenes.

Based on six oxygens, a maximum of 0.026 Al atoms substitutes for silicon among the 17 Voltri omphacites, so essentially all of the aluminum reported in Table 2 is octahedrally coordinated. The sum of $Mg + Fe^{2+}$ is approximately equal in amount to the Ca content, and the $Al + Fe^{3+}$ to the Na content in each

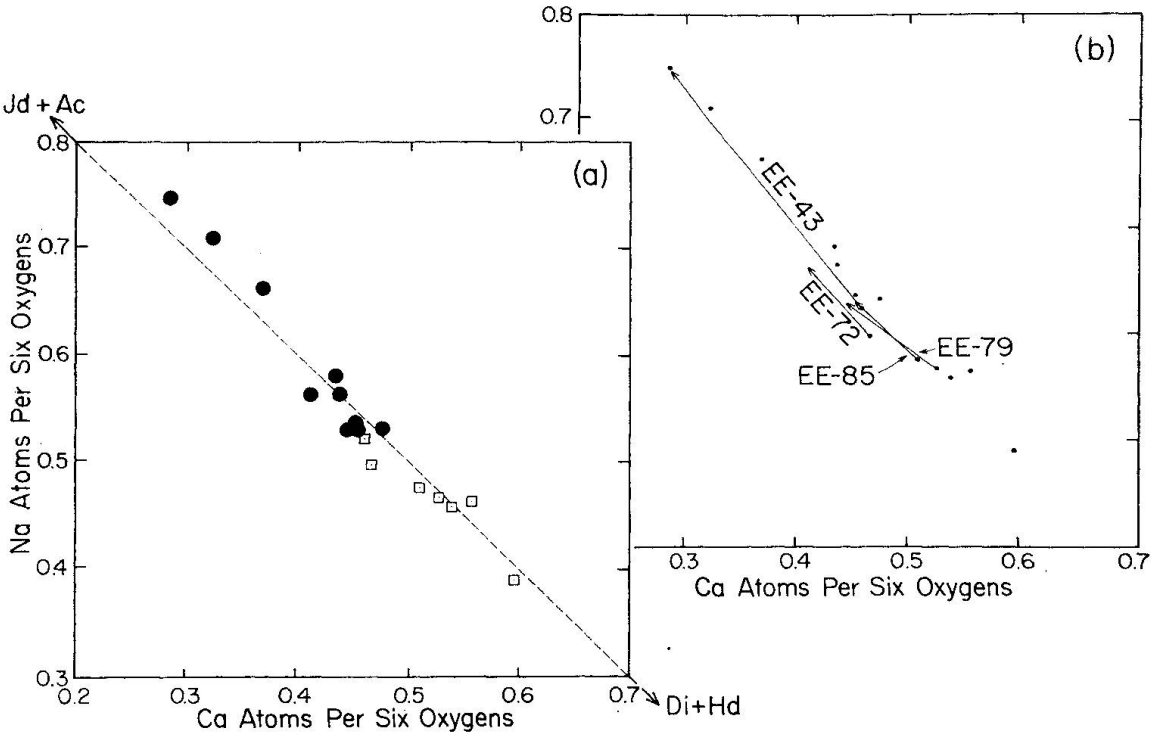

Fig. 5. Proportions of sodium and calcium atoms per formula unit in 17 metamorphic clinopyroxenes from the Voltri eclogitic rocks. The dashed line locates pseudobinary Jd + Ac-Di + Hd compositions in the quaternary system $NaAlSi_2O_6$-$NaFe^{3+}Si_2O_6$-$CaMgSi_2O_6$-$CaFe^{2+}Si_2O_6$. Note that only intermediate Na-Ca solid solutions are shown. The igneous clinopyroxene, EE-28, falls outside the diagram in the lower right-hand corner, and is a subcalcic augite. In (a), filled circles signify stage B omphacites, open squares stage A. In (b), dots indicate Na clinopyroxene analyses, arrows point to stage B compositions for four pairs of A + B omphacites.

pyroxene, but for these chemical relationships to be entirely correct, the exact ferrous-ferric ratios would have to be known and the ideal substitutions to be obeyed. Figure 6 depicts the ternary (Di + Hd)-Jd-Ac and (Jd + Ac)-Hd-Di compositional ranges, and provides an indication of the chemical species occupying the small 6-fold coordinated M_1 site in the Voltri clinopyroxenes. It is clear from this diagram that all the post-mylonitic omphacites contain less Mg, but are more aluminous and possibly also more iron-rich than the stage A sodic clinopyroxenes. Average compositions for the seven stage A omphacites and the ten stage B omphacites are $Jd_{28}Ac_{14}Di_{44}Hd_{14}$ and $Jd_{36}Ac_{17}Di_{30}Hd_{17}$, respectively.

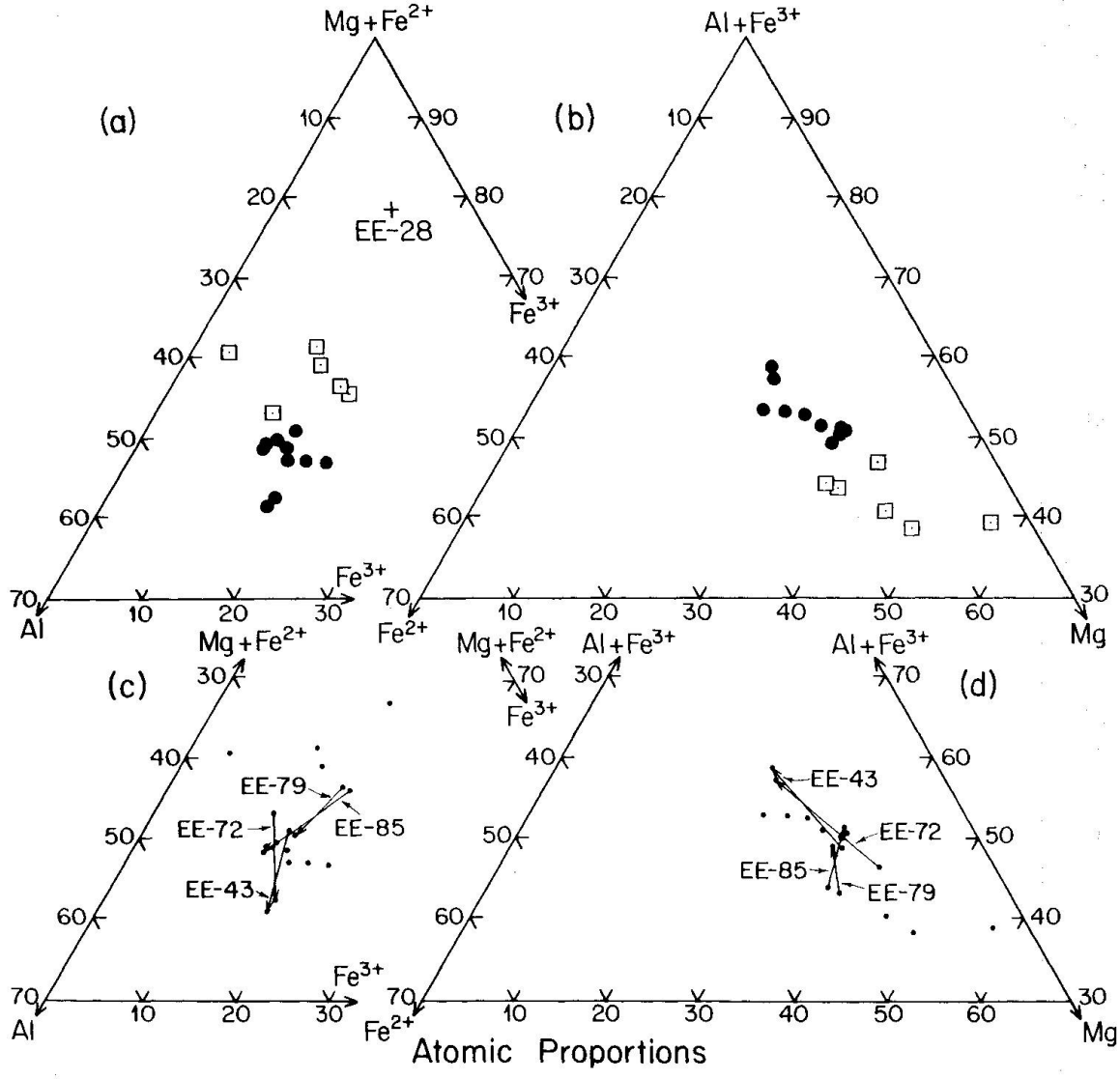

Fig. 6. Ternary atomic proportions of Di + Hd-Jd-Ac (a, c) and of Jd + Ac-Hd-Di (c, d) for clinopyroxenes from the Voltri eclogitic rocks. Note that only the Di + Hd apex in (a), and the Jd + Ac apex in (b) are shown. In (a) and (b), filled circles signify stage B omphacites, open squares stage A; in (a) the cross designates the composition of the single analyzed (subcalcic) igneous augite. In (c) and (d), dots indicate Na clinopyroxene analyses, arrows point to stage B compositions for four pairs of A + B omphacites.

Sodic amphiboles

Analyses for 10 sodic amphiboles are presented in Table 3. Their growth signals recrystallization during stage C. These glaucophane-crossite solid solutions display surprisingly little chemical variation in either major or minor elements. K_2O, MnO, Cr_2O_3 and TiO_2 contents range from 0.01–0.03, 0.00–0.04, 0.00–0.03 and 0.00–0.08 weight percents, respectively. Silica, alumina, total iron oxide and magnesia exhibit comparably small variations percentagewise. Only the CaO contents seem to vary appreciably, between the extremes 0.28–2.31 weight percents. Whether the calcium variation reflects the presence of submicroscopic lamellae of calcic amphibole or not is unknown, but analyses which showed fluctuations in counting rate during sample traversing were discarded; at the compositional resolution level (an area approximately two microns in diameter was excited during electron beam impingement), the sodic amphiboles appear to be homogeneous.

Table 3. *Electron microprobe analyses of sodic amphiboles from eclogitic rocks, Gruppo di Voltri, Ligurian Alps*

	Sample number									
Oxide	EE-3	EE-37	EE-43	EE-63	EE-64	EE-66	EE-77	EE-79	EE-82	EE-85
SiO_2	57.40	55.10	57.69	55.88	56.54	56.10	57.80	57.83	57.93	54.54
Al_2O_3	8.66	7.83	9.33	9.26	9.78	10.58	10.32	9.77	10.63	10.88
TiO_2	0.00	0.00	0.02	0.06	0.02	0.04	0.05	0.02	0.05	0.08
Fe_2O_3	7.25	7.79	6.67	7.47	8.10	8.07	7.09	7.40	7.00	7.87
FeO	6.52	7.01	6.00	6.72	7.30	7.26	6.39	6.67	6.31	7.08
Cr_2O_3	0.00	0.00	0.00	0.00	0.03	0.00	0.00	0.00	0.00	0.00
MgO	9.98	8.24	10.04	9.06	7.85	7.21	9.47	9.25	9.61	8.41
MnO	0.00	0.04	0.02	0.00	0.02	0.00	0.03	0.03	0.03	0.01
CaO	0.28	0.56	0.81	1.67	0.89	0.66	1.10	1.33	1.41	2.31
Na_2O	7.49	6.86	7.16	6.59	7.07	7.23	6.81	6.70	6.78	6.31
K_2O	0.02	0.02	0.03	0.02	0.03	0.01	0.01	0.01	0.02	0.02
H_2O	2.00	2.00	2.00	2.00	2.00	2.00	2.00	2.00	2.00	2.00
Total	99.60	95.45	99.77	98.73	99.63	99.16	101.07	101.01	101.77	99.51

The number of sixfold coordinated $M_1 + M_2 + M_3$ cations per formula unit ranges from 4.779 to 4.926, suggesting that the assumption of a ferrous-ferric ratio of unit value may be too low. The proportions of $(Al + Fe^{3+})$ to $(Mg + Fe^{2+})$ approach $^2/_3$, as in the ideal sodic amphibole structural formula, which to some extent provides support for the assumption of equal quantities of ferrous and ferric iron; however, the sum of octahedrally coordinated aluminum plus ferric iron always exceeds two (values average 2.251) whereas the amount of $Mg + Fe^{2+}$ is invariably less than three (values average 2.622). Compositions in terms of a conventional sodic amphibole quadrilateral are presented in Fig. 7a, and based on total iron-aluminum-magnesium proportions in Fig. 7b. Both diagrams attempt to show the cation occupancy of the $M_1 + M_2 + M_3$ structural sites.

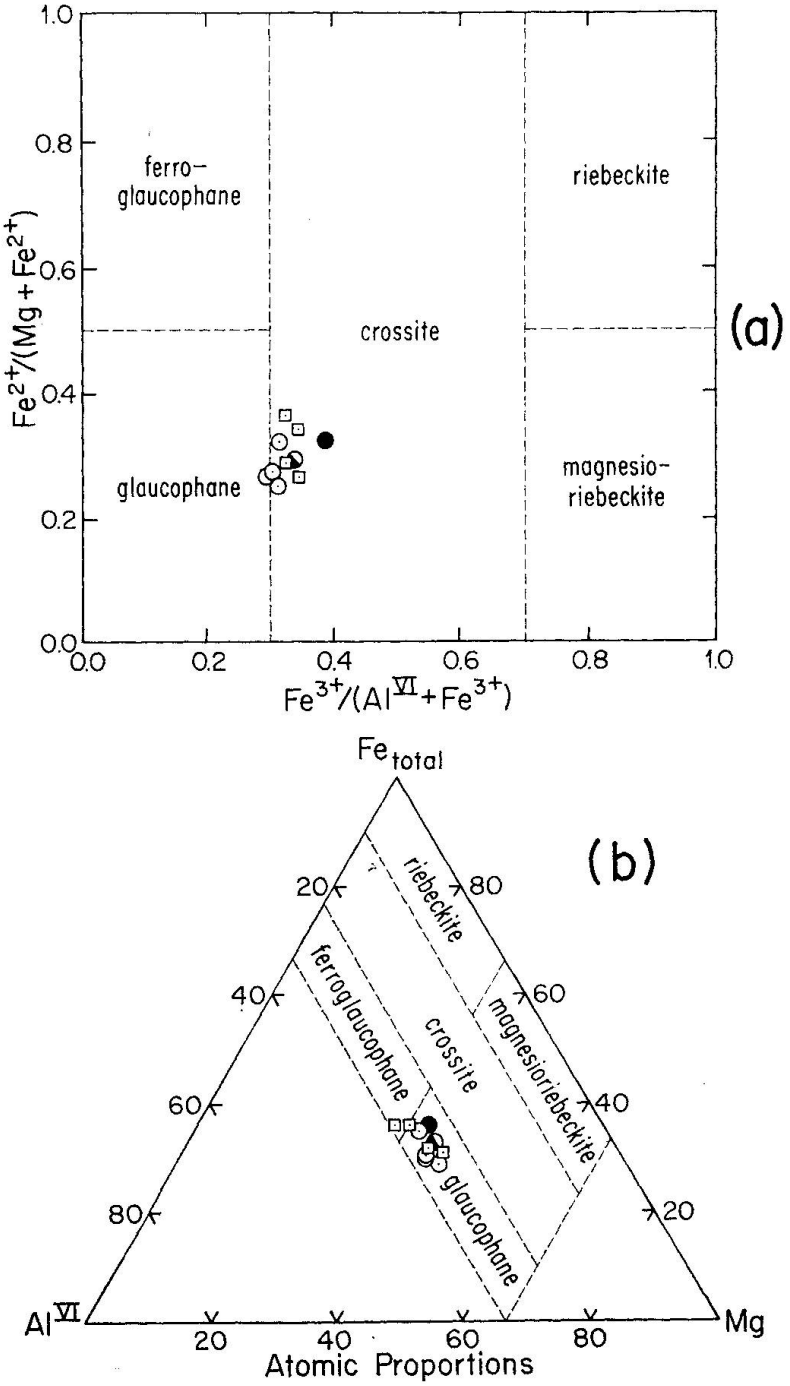

Fig. 7. Compositional range of glaucophanic amphiboles from eclogitic rocks of the Gruppo di Voltri. The classification scheme adopted is slightly modified after MIYASHIRO (1957). Squares designate sodic amphiboles from eclogites which do not contain Ca amphiboles, open and filled circles indicate the presence of actinolitic and barroisitic amphiboles, respectively (divided circle symbolizes the occurrence of both). In both diagrams, only octahedrally coordinated aluminum has been considered. In (a), half of the iron is regarded as ferric, whereas in (b), no assumption regarding the oxidation state of the Na amphibole has been made.

All analyzed Na amphiboles are aluminous crossites and iron-rich glaucophanes in terms of their chemistry according to Fig. 7a. Assuming the general validity of the assumption regarding oxidation state, the compositional data cluster about the approximate pseudobinary value of $Gl_{68}Rieb_{32}$. As evident from Table 3 and Fig. 7a, there seems to be no obvious correlation between the $Fe^{2+}/(Mg+Fe^{2+})$ and/or $Fe^{3+}/(Al^{VI}+Fe^{3+})$ ratios of the sodic amphiboles and their calcium contents or their occurrence in rocks either devoid of calcic amphiboles or, on the contrary, associated with either a barroisitic or an actinolitic phase. There is a faint indication that where the sodic amphiboles are associated with actinolites, they tend to be slightly enriched in Gl, but the small number of analyses precludes a more definitive statement.

If we retain the assumption regarding the ferrous-ferric ratios of the sodic amphiboles for the purpose of calculating tetrahedral and octahedral cation proportions, but plot the analyzed $Al^{VI}+Fe_{total}+Mg$ ratios as in Fig. 7b, the phases appear to be iron-rich glaucophanes bordering on ferroglaucophane in chemistry; the aluminum contents plotted include only six-fold coordinated cations, a correction having been made for tetrahedral Al which averages 0.138 atoms per formula unit. According to Fig. 7b, the proportions of ferrous iron to some extent outweigh the ferric, and the analyses cluster around the ternary composition of $Gl_{60}Fe\text{-}Gl_{24}Rieb_{16}$. As with Fig. 7a, however, there seems to be no clear relationship between amphibole Fe-Al-Mg ratio and either Ca content or occurrence, although a weak grouping suggests that the most aluminous glaucophanes are those which are associated with actinolitic amphibole.

Calcic amphiboles

Analytical data for 21 calcic amphiboles are presented in Table 4. Of these, eleven are classified as Al-bearing actinolites (two of which, EE-63 and EE-63′, are replicate analyses performed on grains from different portions of the same probe mount), and the others are barroisites and blue-green hornblendes intermediate in composition between barroisite and actinolite. In the table, the aluminous actinolites are designated act, barroisites and intermediate hornblendes hb, the former having crystallized in stage E, the latter more or less confined to stage D. It should be noted that two rocks, EE-37 and EE-93, classified as greenschists by Cortesogno et al. (in press, Table 9) contain calcic amphiboles which, on electron microprobe analysis, appear to represent intermediate actinolite-barroisite solid solutions. Any classification scheme of this sort will possess a degree of arbitrariness, and what is important is the fact that the calcic amphibole continuously changes composition passing from stage D to E, as will be shown below.

In general, chromium oxide contents of the clinoamphiboles are quite low,

Table 4. *Electron microprobe analyses of calcic amphiboles from eclogitic rocks, Gruppo di Voltri, Ligurian Alps*

	Sample number										
Oxide	EE-12 hb	EE-17 act	EE-24 hb	EE-27 hb	EE-28 act	EE-28 hb	EE-31 hb	EE-33 act	EE-37 hb	EE-43 act	EE-59 hb
SiO_2	47.20	53.42	50.86	44.85	53.59	40.94	44.72	52.86	45.74	54.73	42.63
Al_2O_3	8.54	3.71	6.71	8.27	2.67	11.46	10.62	3.40	7.32	3.63	12.46
TiO_2	0.11	0.09	0.22	0.25	0.03	0.24	0.25	0.06	0.14	0.08	0.21
FeO	12.99	6.79	17.93	10.67	11.84	14.93	19.79	12.64	19.71	11.62	23.12
Cr_2O_3	0.03	0.08	0.48	0.00	0.00	0.02	0.00	0.00	0.00	0.00	0.00
MgO	12.31	17.38	14.22	10.15	14.84	11.02	7.80	13.98	7.40	15.36	5.48
MnO	0.25	0.24	0.23	0.22	0.14	0.25	0.14	0.22	0.39	0.05	0.16
CaO	11.20	12.37	10.73	10.14	10.42	11.03	8.73	10.37	7.64	8.68	7.48
Na_2O	2.23	1.30	2.54	3.37	1.49	3.35	3.75	1.11	3.38	3.62	4.79
K_2O	0.35	0.06	0.14	0.18	0.05	0.23	0.27	0.07	0.22	0.06	0.35
H_2O	2.00	2.00	2.00	2.00	2.00	2.00	2.00	2.00	2.00	2.00	2.00
Total	97.21	97.43	98.79	97.37	97.06	95.47	98.07	96.71	93.94	99.84	98.69

	Sample number									
Oxide	EE-63 act	EE-63′ act	EE-63 hb	EE-72 hb	EE-73 act rim	EE-74 act	EE-77 act	EE-85 act	EE-90 act	EE-93 hb
SiO_2	54.80	55.03	46.14	40.29	52.95	57.92	55.92	55.63	53.79	50.12
Al_2O_3	2.45	2.19	10.91	13.02	4.75	2.83	3.03	3.29	5.37	6.09
TiO_2	0.02	0.00	0.25	0.51	0.06	0.06	0.24	0.05	0.08	0.15
FeO	12.08	11.70	17.54	24.28	9.34	4.00	11.97	10.71	10.46	17.76
Cr_2O_3	0.00	0.00	0.00	0.00	0.00	0.02	0.00	0.00	0.00	0.01
MgO	14.96	15.46	8.52	5.00	16.66	21.52	15.59	16.12	16.17	11.74
MnO	0.05	0.04	0.07	0.24	0.22	0.09	0.07	0.03	0.19	0.34
CaO	9.47	9.74	8.08	8.10	9.85	12.11	9.42	9.57	10.31	9.05
Na_2O	2.18	1.85	4.01	4.55	2.28	0.79	2.12	2.15	1.85	1.80
K_2O	0.07	0.04	0.29	0.66	0.13	0.04	0.02	0.02	0.11	0.23
H_2O	2.00	2.00	2.00	2.00	2.00	2.00	2.00	2.00	2.00	2.00
Total	98.07	98.06	97.81	98.65	98.24	101.37	100.38	99.58	100.32	99.30

except for sample EE-24 which contains 0.48 weight percent Cr_2O_3. MnO ranges between 0.04 and 0.39 weight percent, with actinolites and hornblendes averaging 0.12 and 0.23, respectively. Weight percent averages for other minor elements are: for TiO_2, actinolite = 0.09, hornblende = 0.23; and for K_2O, actinolite = 0.06, hornblende = 0.29. The other six major elements, for which analyses were obtained in this study, namely Si, Al, Fe, Mg, Ca and Na, show important variations, as discussed below. As mentioned previously, all iron was treated as ferrous for simplicity.

Ignoring the small amounts of potassium located in the twelvefold coordinated structural site, and the minor iron + manganese + magnesium situated in the eightfold coordinated M_4 sites (an excess of octahedrally coordinated atoms occurs in 17 of the 21 samples, and in these 17 averages 0.125 atoms per formula unit over the ideal value of 5.0), the Na and Ca occupants of $M_4 + A$ are shown in Fig. 8. It is clear that the precurser barroisitic amphiboles and blue-green hornblendes contain appreciably more sodium but similar amounts of calcium compared to the later actinolitic amphiboles. This penomenon is also

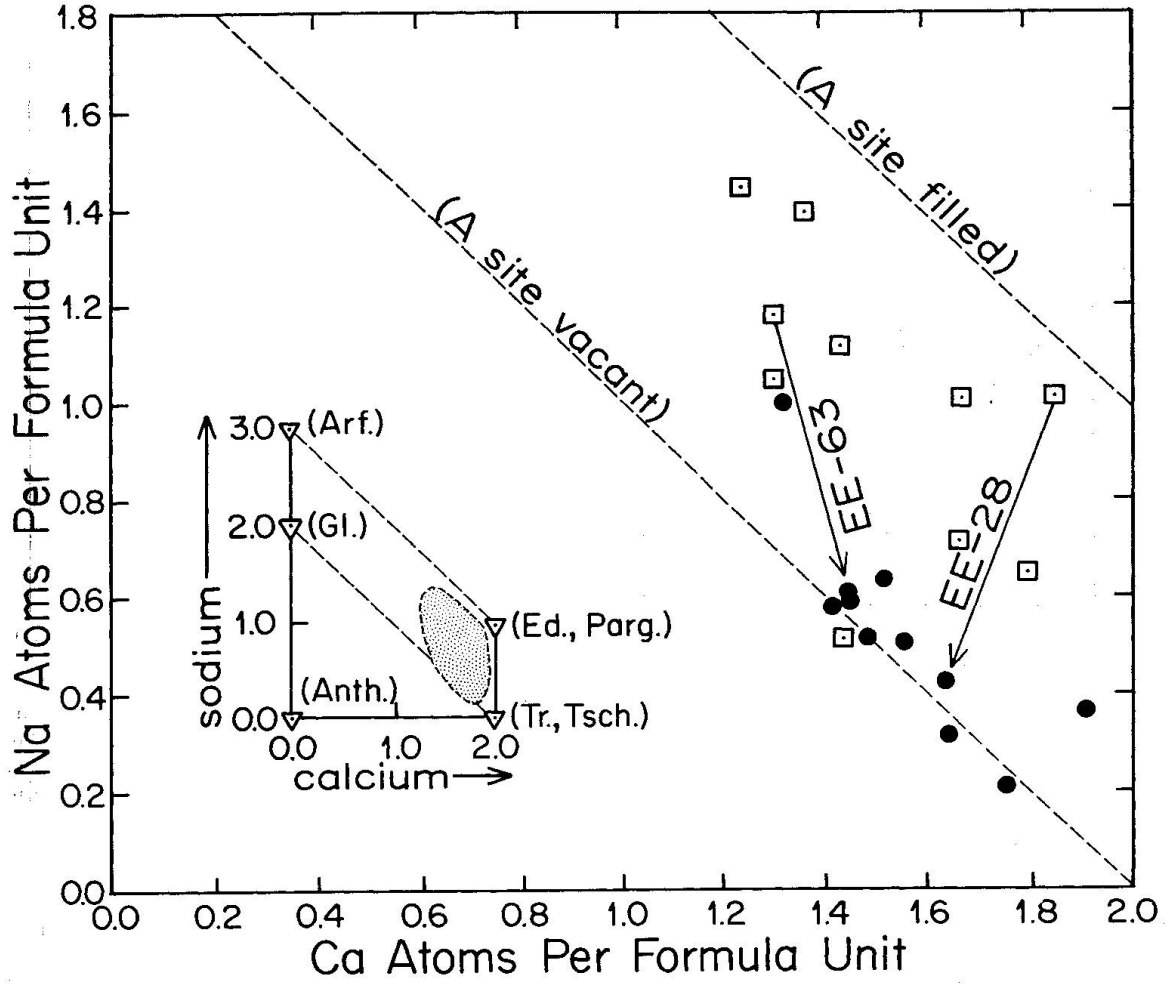

Fig. 8. Proportions of sodium and calcium atoms per formula unit in 21 calcic amphiboles from the Voltri eclogitic rocks. Open squares designate barroisitic amphiboles and blue-green hornblendes, filled circles denote aluminous actinolites. Ca and Na proportions for pairs of analyzed barroisite + actinolite are also illustrated, with arrows pointing to the later phases. The inset shows possible Ca + Na variations in A + M_4 structural site occupancy, the compositional range of analyzed calcic clinoamphiboles from the Gruppo di Voltri (stippled), and some Mg ± Al end members, including the hypothetical MgAl equivalent of arfvedsonite (filled triangles).

reflected in the data for pairs of analyses from samples EE-28 and EE-63, each of which contain both early barroisite and late prasinitic amphibole. All 21 clinoamphiboles are subcalcic, containing between 1.245 and 1.906 calcium atoms and averaging 1.535 per formula unit. They may therefore be considered as complex Tr-Gl-Parg solid solutions. The small inset in Fig. 8 is schematic, but more complete, and illustrates the classical Ca and Na substitutions of amphiboles, as well as some Mg + Al end member compositions in terms of the chosen coordinates.

Figure 9 attemps to show the proportions of aluminum, magnesium and total iron residing in the $M_1 + M_2 + M_3$ structural sites, as a function of the number of Si atoms per formula unit. A reciprocal relationship would be obtained for

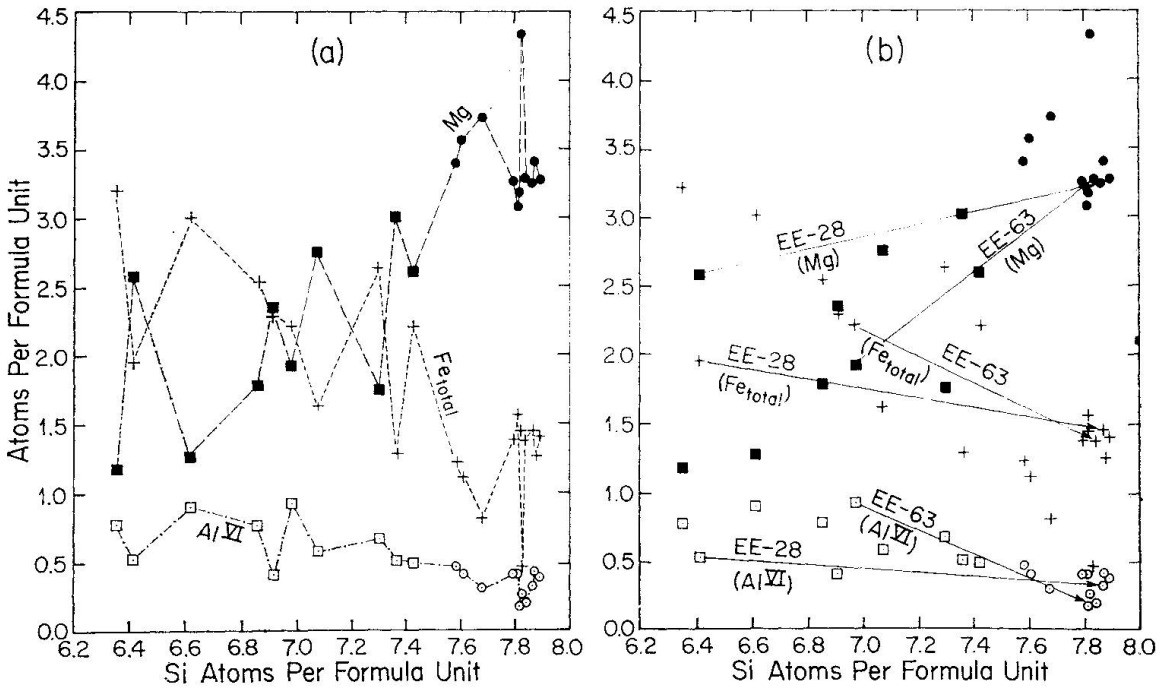

Fig. 9. Variations in magnesium, total iron and octahedrally coordinated aluminum as a function of the number of Si^{IV} atoms per formula unit for calcic amphiboles from the Voltri Massif. For Mg and Al^{VI}, squares symbolize barroisitic compositions, circles indicate actinolites. The lines connecting all analytical data for a specific element in (a) have no particular significance except to guide the eye in discerning the overall chemical trends. Compositions for two analyzed barroisite + actinolite pairs are shown in (b), with arrows pointing to the later phases.

the depicted atomic proportions as a function of tetrahedrally coordinated aluminum. Note that, whereas the analyzed barroisites and blue-green hornblendes of intermediate composition range in Si contents from 6.354 to 7.427, the actinolites are more markedly grouped with respect to this parameter, and range only from 7.584 to 7.889 Si per formula unit. As previously mentioned, and as can be seen from Fig. 9a, the sum of octahedrally coordinated cations closely approaches the ideal value, but in general is slightly greater than 5.0. If some of the iron were recast as ferric, the amount of tetrahedrally coordinated aluminum would increase at the expense of Al^{VI} reflecting a diminution in the metal/oxygen ratio, and the cation excess of $M_1 + M_2 + M_3$ would be correspondingly reduced. The Fe/Mg ratios of the clinoamphiboles is chiefly a function of host rock chemistry, and to a lesser extent, physical conditions of metamorphism; a faint tendency towards more magnesian compositions can be discerned among the more actinolitic members of the series (CORTESOGNO et al., in press, showed that, in general, the prasinites have lower bulk Fe/Mg ratios than the amphibolites). The amount of Al^{VI} also is slightly less in the more greenschistic amphiboles. In spite of rather diverse compositions of the earlier barroisites in samples EE-28 and EE-63, the late actinolite seems to be rather similar in both cases with regard to Si^{IV}, Al^{IV}, Al^{VI}, total Fe and Mg contents.

Epidote group minerals

The compositions of 16 epidotes and epidote-clinozoisite solid solutions are presented in Table 5. Because the onset of epidote crystallization marked the wholesale destruction of garnet – both rims as well as cores – epidote group minerals crystallized only towards the end of the glaucophanitic stage and principally during the formation of barroisitic amphibolites and the later greenschists (stages D and E, respectively). Where hornblende is well preserved in the rock, analyses of epidote group minerals probably reflect the compositional range of this phase during stage D growth; in contrast, in rock samples containing aluminous actinolite as the major or sole amphibole, the chemical data for epidote group minerals probably represent the composition of the stable phase during the stage E production of greenschists. Of course, this is simply a plausibility argument which need not be correct in detail due to the preservation of metastable relics of amphibole or epidote. Nevertheless the occurrence

Table 5. *Electron microprobe analyses of epidote group minerals from eclogitic rocks, Gruppo di Voltri, Ligurian Alps*

	Sample number							
Oxide	EE-12 hb	EE-17 act	EE-24 hb	EE-27 hb	EE-28 hb+act	EE-31 hb	EE-33 act	EE-37 hb
SiO_2	38.40	39.03	38.02	37.65	37.50	37.81	39.99	37.70
Al_2O_3	26.90	32.71	26.21	23.49	23.01	24.22	28.17	24.21
TiO_2	0.06	0.02	0.16	0.05	0.08	0.08	0.16	0.04
Fe_2O_3	7.83	0.71	8.85	12.54	13.21	12.04	6.81	11.88
Cr_2O_3	0.02	0.00	0.16	0.01	0.00	0.00	0.00	0.00
MgO	0.19	0.00	0.04	0.02	0.02	0.10	0.03	0.04
MnO	0.09	0.05	0.19	0.16	0.17	0.11	0.11	0.07
CaO	22.45	25.63	24.71	22.26	22.25	22.49	22.85	22.23
Na_2O	0.04	0.01	0.01	0.00	0.01	0.00	0.00	0.00
K_2O	0.01	0.00	0.00	0.00	0.00	0.00	0.00	0.00
H_2O	2.00	2.00	2.00	2.00	2.00	2.00	2.00	2.00
Total	97.99	100.16	100.35	98.18	98.25	98.85	98.12	98.17

	Sample number							
Oxide	EE-41	EE-59 hb	EE-72 hb	EE-73 act	EE-74 act	EE-90 act	EE-93 hb	EE-95
SiO_2	37.58	37.91	37.01	38.23	38.31	38.19	38.60	37.97
Al_2O_3	23.63	24.70	24.33	28.39	30.81	28.86	26.14	26.29
TiO_2	0.09	0.07	0.15	0.25	0.08	0.12	0.05	0.10
Fe_2O_3	12.38	13.10	13.39	8.35	5.29	8.65	12.11	11.49
Cr_2O_3	0.02	0.00	0.00	0.06	0.03	0.00	0.04	0.05
MgO	0.01	0.03	0.02	0.04	0.06	0.07	0.02	0.04
MnO	0.22	0.18	0.21	0.21	0.04	0.21	0.20	0.19
CaO	22.60	22.40	22.60	23.02	23.53	23.35	22.74	22.90
Na_2O	0.00	0.00	0.00	0.00	0.00	0.01	0.02	0.00
K_2O	0.00	0.00	0.00	0.00	0.00	0.00	0.00	0.00
H_2O	2.00	2.00	2.00	2.00	2.00	2.00	2.00	2.00
Total	98.53	100.39	99.71	100.55	100.15	101.46	101.92	101.03

and nature of associated amphiboles ($\approx$ reflecting the stage of epidote formation?) is indicated in Table 5.

Examination of the analytical data shows that potassium is not present in the epidotes, and sodium is either absent or present as a minor element (Na_2O averages just 0.02 weight percent in the six samples in which it was detected). Other analyzed minor oxides all show low but relatively constant values in all 16 samples. Weight percent averages for TiO_2, Cr_2O_3, MgO and MnO are 0.10, 0.03, 0.05 and 0.15, respectively. Of the remaining oxides, silica and lime exhibit reasonably small variations: the former ranges between 37.01 and 39.03 weight percent, and the latter between 22.23 and 25.63 weight percent.

The aluminum is essentially all 6-fold coordinated in the analyzed epidote group minerals: of 10 specimens containing Al^{IV} in the 3 tetrahedral sites, the maximum amount calculated per formula unit is only 0.065, and the average is of course much less. Ferric iron and aluminum exhibit a reciprocal concentration relationship as shown in Fig. 10. The closeness with which the analytical data conform to the line $\sum(Al + Fe^{3+})^{VI} = 3.0$ indicates, as does Table 5, that these minerals are essentially binary Pist-Zo solid solutions (where Pist =

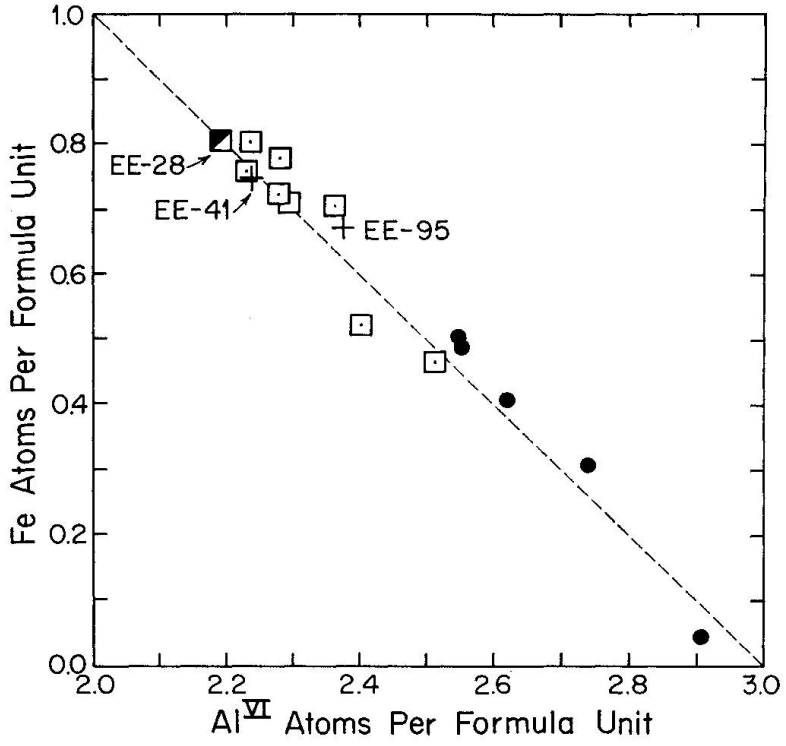

Fig. 10. Proportions of octahedrally coordinated aluminum and ferric iron in epidote group minerals from the Voltri eclogitic rocks in the system Pist (Fe^{3+} = 1.0, Al = 2.0)-Zo (Fe^{3+} = 0.0, Al = 3.0). Symbols for epidote host rocks are as follows: filled circles = actinolitic greenschists; crosses = greenschists devoid of calcic amphiboles; open squares = barroisitic amphibolites; half-filled square = prasinitized amphibolite characterized by the occurrence of both barroisite and actinolite.

1.0 Fe^{3+}, 2.0 Al). As seen from the figure, epidote group minerals associated with actinolite (stage E) tend to be enriched in Al relative to Fe^{3+}, hence are clinozoisitic, whereas in the barrositic amphibolite stage (D), more pistacitic compositions of epidote were produced. The latter average approximately $Pist_{65}Zo_{35}$, whereas the former roughly average $Pist_{30}Zo_{70}$. This mineralogic contrast may in part reflect the more magnesian nature of the prasinites, as documented by CORTESOGNO et al. (in press). Samples EE-41 and EE-91 are prasinites lacking calcic amphibole, so the compositions of these epidotes are not constrained to be similar to those occurring in actinolitic greenschists. Where faint compositional zoning has been detected in some epidote grains, the core is invariably richer in iron than the rim; thus within a single specimen, as well as from comparison of different metamorphic phase assemblages, it is clear that epidote became progressively more aluminous while growth took place during the transition of physical conditions from stage D to E. Thus the difference in composition of epidotes from amphibolites and greenschists must in part reflect disparate physical conditions.

Chlorite

Analyses of 13 chlorites, roughly half of which occur in barroisitic amphibolites and the other half in greenschists, are presented in Table 6. Chlorite evidently crystallized during both stage D and stage E. Most of the oxide totals are substantially less than 100 percent, casting suspicion on the quality of the data. Nevertheless, based on one formula unit, chlorite cation sums range between 9.949 and 9.991, averaging 9.969, in astonishingly good agreement with the ideal value of 10.0. Possibly the assumed H_2O content of 12.0 weight percent is insufficient, which would help to account for the low oxide totals listed.

Table 6. *Electron microprobe analyses of chlorites from eclogitic rocks, Gruppo di Voltri, Ligurian Alps*

	Sample number												
Oxide	EE-12 hb	EE-17 act	EE-24 hb	EE-28 act/hb	EE-33 act	EE-37 hb	EE-41	EE-59 hb	EE-63 act/hb	EE-74 act	EE-90 act	EE-93 hb	EE-95
SiO_2	27.27	28.40	27.32	27.47	25.53	25.42	24.38	24.44	24.98	28.09	27.56	25.53	26.05
Al_2O_3	20.18	19.15	20.35	18.82	19.46	20.14	19.74	21.38	21.56	22.43	20.62	22.44	21.95
TiO_2	0.00	0.00	0.00	0.00	0.00	0.13	0.11	0.05	0.02	0.00	0.02	0.12	0.10
FeO	16.24	10.13	15.15	13.57	23.36	22.19	25.52	27.73	25.38	6.25	18.32	20.92	22.05
Cr_2O_3	0.01	0.40	0.00	0.00	0.00	0.00	0.00	0.00	0.00	0.04	0.00	0.02	0.03
MgO	21.51	25.33	21.69	22.76	15.77	16.09	13.11	12.52	13.99	28.94	21.12	17.30	17.64
MnO	0.25	0.17	0.22	0.23	0.21	0.35	0.15	0.42	0.09	0.08	0.16	0.68	0.38
CaO	0.05	0.40	0.05	0.03	0.03	0.03	0.03	0.03	0.03	0.02	0.03	0.02	0.03
Na_2O	0.00	0.01	0.00	0.00	0.00	0.01	0.01	0.02	0.00	0.00	0.00	0.01	0.00
K_2O	0.00	0.01	0.00	0.00	0.00	0.00	0.00	0.00	0.00	0.00	0.00	0.15	0.02
H_2O	12.00	12.00	12.00	12.00	12.00	12.00	12.00	12.00	12.00	12.00	12.00	12.00	12.00
Total	97.51	96.02	96.79	94.88	96.35	96.35	95.05	98.54	98.06	97.85	99.84	99.19	100.25

As evident from Table 6, the weight percents of minor oxides show small and reasonably constant average values as follows: $TiO_2 = 0.04$; Cr_2O_3 and $CaO = 0.01$ and 0.03, respectively (except for one sample which contains 0.40 weight percent of each constituent); and $MnO = 0.26$. Alkali contents are negligible.

The major oxides SiO_2 and Al_2O_3 display relatively uniform values in the chlorites, the former ranging from 24.38 to 28.40 weight percent and the latter from 18.82 to 22.44. However, Si and Al must bear an inverse concentration relationship to one another judging from Fig. 11a. Here it is shown that the tetrahedrally and octahedrally coordinated aluminum are virtually equal in proportion – hence the total Al increases at twice the rate of Si decrease and vice versa. In Fig. 11a it appears that the amount of 6-fold coordinated aluminum actually exceeds that of Al^{IV}, but the absolute difference is small (averaging 0.053 atoms per formula unit), and seems to be unrelated to the inferred stages of crystallization of the chlorite.

The variation of iron/magnesium ratio, as a function of silicon content per formula unit, and the nomenclatural scheme for chlorites are illustrated in Fig. 11b. Clearly a wide range of Fe-Mg(-Al^{VI}) proportions is represented in the chlorites, but apparently the phase chemistry was controlled chiefly by parental rock bulk composition, with no discernible influence exerted by the disparate

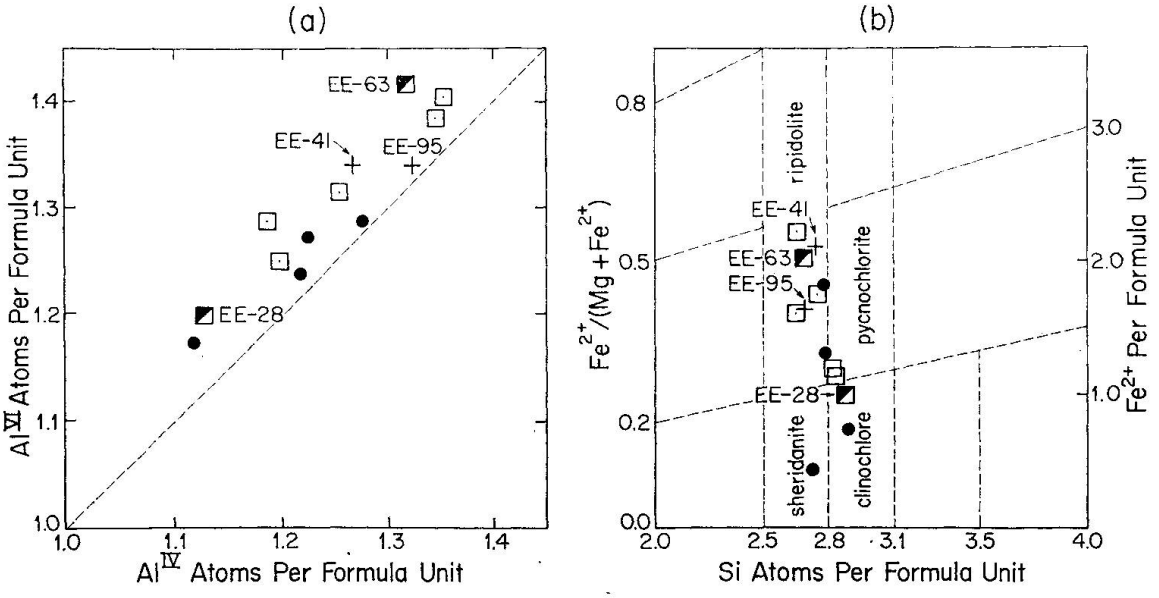

Fig. 11. Compositional range of chlorites from the Voltri eclogitic rocks; numbers of atoms are based on one formula unit (10 metal atoms exclusive of hydrogen). Symbols designate the host schists: filled circles = actinolitic greenschists; crosses = greenschists devoid of calcic amphiboles; open squares = barroisitic amphibolites; half-filled squares = prasinitized amphibolites containing both barroisitic and actinolitic amphibole. (a) Illustrates proportions of four- and six-fold coordinated aluminum; the dashed line indicates equal amounts of aluminum in both types of structural site, and represents serpentine-clinochlore-corundophylite type substitution. (b) Classification of chlorites after HEY (1954), with the proviso that all iron present is divalent.

physical conditions which presumably characterized stages D and E. The Voltri chlorites in general are intermediate members of the clinochlore-daphnite solid solution series and are most appropriately termed ripidolites.

Sodic plagioclases

Analyses of 13 Na plagioclases are listed in Table 7; roughly half are associated with barroisitic hornblendes, whereas the remainder occur in prasinites. Except for sample EE-74, a greenschist, the premetamorphic lithology of which was rodingitic judging from the bulk chemical analyses (CORTESOGNO et al., in press), all the samples are nearly pure albite. The contents of TiO_2, Cr_2O_3, MgO and MnO are negligible, and in aggregate only average 0.01 total weight percent. Potash contents are rather constant, range from 0.02 to 0.09 and average a little more than 0.03 weight percent. Ferric iron seems to be slightly more abundant in stage D (?) plagioclase associated with hornblende (average of seven = 0.20 weight percent Fe_2O_3) compared to greenschistic plagioclase (average of six = 0.10 weight percent Fe_2O_3), but the ranges overlap considerably and the differences may not be significant. Based on one formula unit, plagioclase cation sums range from 4.988 to 5.012 and average 4.995, in excellent agreement with the ideal value of 5.0.

The An content of the plagioclase may be calculated in a variety of ways, one of which is shown graphically in Fig. 12a; here the cation proportions in the large structural site are shown. Employing sodium-calcium-potassium proportions, eleven of the analyzed plagioclases display a remarkably restricted compositional range, $Ab_{97.8-99.6}An_{0.3-2.1}Or_{0.1-0.2}$, whereas a twelfth, sample EE-12, is closely similar as $Ab_{96.0}An_{2.3}Or_{1.7}$. In terms of alkalis and calcium proportions, the plagioclase from metarodingitic greenschist EE-74 has the

Table 7. *Electron microprobe analyses of sodic plagioclases from eclogitic rocks, Gruppo di Voltri, Ligurian Alps*

	Sample number												
Oxide	EE-12 hb	EE-17 act	EE-24 hb	EE-27 hb	EE-31 hb	EE-33 act	EE-37 hb	EE-41	EE-59 hb	EE-72 hb	EE-73 act	EE-74 act	EE-90 act
SiO_2	68.67	67.55	68.87	68.63	69.08	68.30	68.93	68.62	68.32	69.56	69.89	66.15	70.66
Al_2O_3	19.27	18.55	19.43	19.19	18.87	18.98	18.74	18.52	20.60	19.87	20.03	24.02	20.26
TiO_2	0.00	0.00	0.00	0.00	0.00	0.00	0.00	0.00	0.00	0.00	0.00	0.02	0.02
Fe_2O_3	0.19	0.04	0.05	0.08	0.29	0.11	0.23	0.07	0.31	0.23	0.08	0.09	0.20
Cr_2O_3	0.00	0.00	0.02	0.01	0.00	0.00	0.00	0.00	0.02	0.00	0.00	0.00	0.00
MgO	0.02	0.04	0.00	0.00	0.01	0.00	0.00	0.00	0.00	0.00	0.01	0.00	0.00
MnO	0.00	0.01	0.00	0.00	0.00	0.00	0.00	0.00	0.00	0.00	0.00	0.00	0.00
CaO	0.52	0.29	0.44	0.45	0.24	0.37	0.16	0.10	0.56	0.19	0.25	4.54	0.21
Na_2O	11.77	11.45	11.62	11.81	11.96	11.69	11.94	11.74	11.57	11.63	11.32	9.04	11.62
K_2O	0.03	0.02	0.02	0.02	0.02	0.04	0.03	0.02	0.03	0.04	0.04	0.09	0.05
Total	100.46	97.95	100.45	100.20	100.46	99.48	100.02	99.05	101.41	101.52	101.62	103.95	103.02

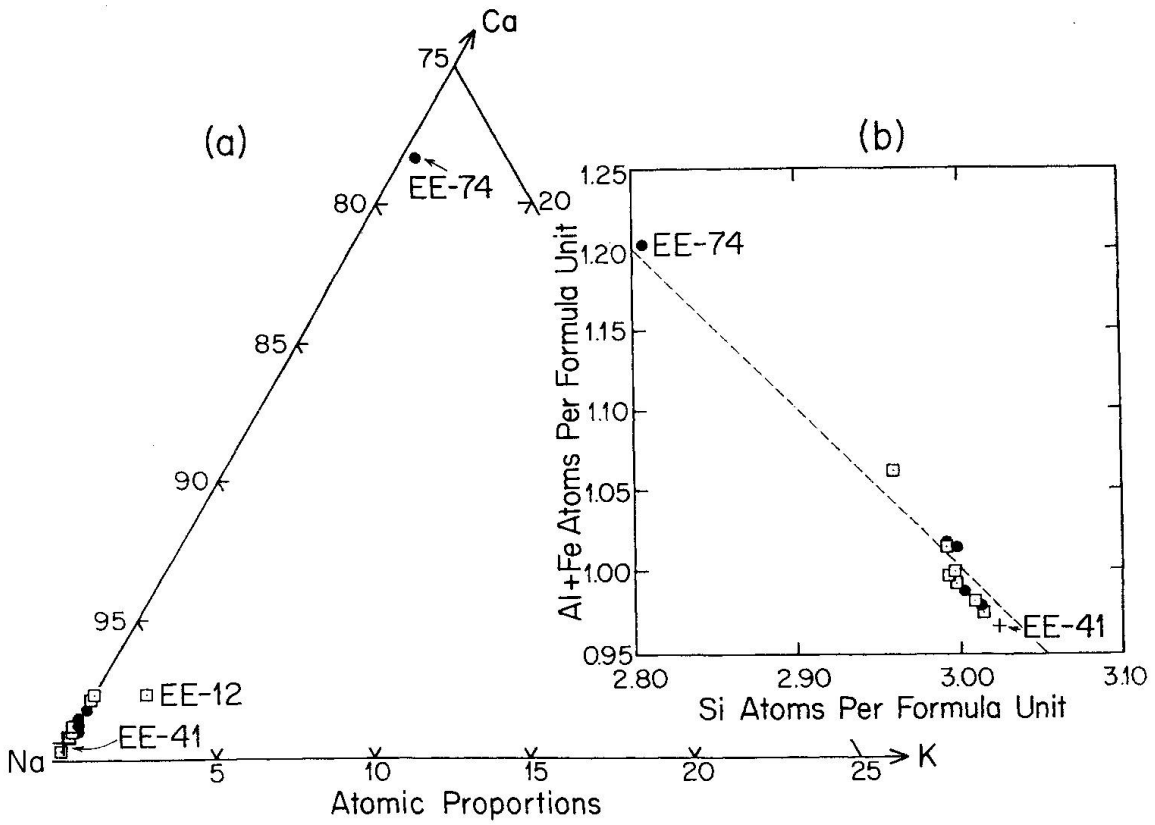

Fig. 12. Proportions of (a) Na-Ca-K and of (b) Si-(Al+Fe^{3+}) for plagioclases from the Gruppo di Voltri. Symbols designate the host rocks as follows: filled circles = actinolitic greenschists; cross = prasinite lacking amphibole; open squares = barroisitic amphibolites. Note that only the Ab apex of the ternary feldspar diagram is shown in (a). The dashed line in (b) indicates the ideal feldspar tetrahedral site occupancy assuming that silicon, aluminum and ferric iron are the only four-fold coordinated atoms.

strongly contrasting composition $Ab_{77.9}An_{21.6}Or_{0.5}$. The chemical data are shown on a plot of the number of tetrahedrally coordinated Si versus Al + Fe^{3+} in Fig. 12b; the closeness with which the analyses coincide with the line defined by the relationship $\sum Si + Al + Fe^{3+} = 4$ is a measure of the approach of the tetrahedral site population to the ideal feldspar formula. Some of the more siliceous samples display a very slight deficiency of Na + Ca + K, compatible with charge balance requirements, but whether this effect is real or merely reflects imprecision in the analyses is not known. In any case, the apparent Si excess is quite small, being 0.023 atoms or less per formula unit. No systematic trend of plagioclase compositions as a function of mineral assemblage – and P-T conditions – is discernible in Fig. 12. On the contrary, plagioclase composition tends to reflect the bulk rock chemistry: for instance, oligoclase occurs in the highly calcic sample EE-74, whereas EE-41 (a quartz keratophyric whole rock composition and the only felsic rock of the 83 analyzed by Cortesogno et al., in press) lacks Ca amphibole entirely and carries virtually pure albite.

Micas

Analytical data for two paragonites, two phengites and three biotites are listed in Table 8 (and abbreviated pa, ms and bi, respectively). Because of the limited number of analyses, it would be inappropriate to discuss the analyses in detail, but several tentative generalizations can be made regarding phase chemistry. The biotites contain appreciable amounts of TiO_2 and MnO, averaging 1.55 and 0.20 weight percents, respectively, whereas these oxides occur in negligible concentrations in the white micas. Paragonites carry much less MgO + FeO (average = 0.21 + 0.81 weight percents, respectively) than do the phengites (average = 5.10 + 2.79 weight percents, respectively). Both paragonite and biotite contain small amounts of calcium (CaO averages 0.09 weight percent) whereas the two analyzed phengites contain none. The dioctahedral nature of the four white micas is reflected in totals for sixfold coordinated cat-

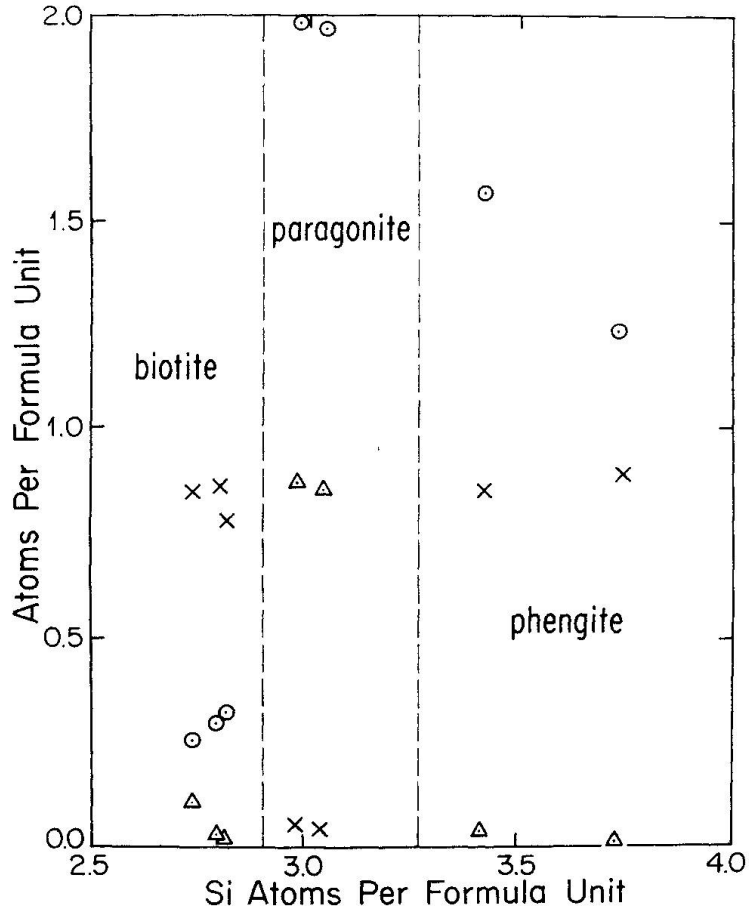

Fig. 13. Variations in octahedrally coordinated aluminum (open circles), and in the interlayer species potassium (Xs) and sodium (open triangles) as a function of the number of Si^{IV} atoms per formula unit, for micas from the Voltri Massif. The vertical dashed lines separating biotites, paragonites and phengites are meant to lead the eye to the chemical contrasts among the phases, not to represent compositional limits of these minerals.

Table 8. *Electron microprobe analyses of micas from eclogitic rocks, Gruppo di Voltri, Ligurian Alps*

Oxide	Sample number EE-41 pa	EE-72 bi	EE-73 pa	EE-74 ms	EE-93 bi	EE-95 bi	EE-95 ms
SiO_2	46.18	35.05	46.56	53.24	36.85	36.70	56.76
Al_2O_3	37.73	16.41	39.75	28.49	16.77	16.67	19.49
TiO_2	0.03	0.59	0.00	0.20	2.19	1.87	0.10
FeO	0.94	18.31	0.69	1.45	17.34	17.84	4.13
Cr_2O_3	0.00	0.00	0.00	0.12	0.01	0.05	0.02
MgO	0.16	13.02	0.47	4.19	11.99	11.78	6.02
MnO	0.00	0.13	0.00	0.00	0.27	0.18	0.00
CaO	0.16	0.05	0.08	0.00	0.07	0.11	0.00
Na_2O	6.71	0.63	7.00	0.31	0.10	0.08	0.01
K_2O	0.41	8.47	0.56	10.36	8.94	7.92	10.66
H_2O	4.00	4.00	4.00	4.00	4.00	4.00	4.00
Total	96.32	96.65	99.12	102.36	98.52	97.19	101.18

ions which, based on one formula unit, range between 2.038 and 2.063, averaging 2.054; for the trioctahedral biotites, the comparable sums range from 2.888 to 3.001 and average 2.939 – again showing a close approach to the ideal formula.

Variations of Al^{VI} and alkalis as a function of the number of tetrahedrally coordinated silicon atoms are presented in Fig. 13, which also illustrates the contrasts in Si (and Al^{IV}) atoms per formula unit for the three different types of mica. There are of course insufficient data for each mineral species to quantitatively relate its chemistry to the phase assemblage and stage of formation.

Sphenes

For completeness, analyses of three sphenes performed during this study are presented in Table 9. Two are associated with barroisitic hornblendes (stage D), whereas the third occurs in a greenschist which lacks amphibole (stage E). The data exhibit relatively constant proportions of the major oxides SiO_2, TiO_2 and CaO, as well as modest quantities of alumina and ferrous oxide. Weight percent ranges are as follows: SiO_2, 30.77–31.34; TiO_2, 36.36–40.95; CaO, 27.21–27.77; Al_2O_3, 0.84–2.47, and FeO, 0.34–0.42. All other analyzed elements occur in insignificant amounts. In spite of departures of the oxide sums from 100 percent, the cation proportions of sphene based on one formula unit total between 2.996 and 3.010 (the average of the three is 3.004), in good agreement with the ideal value of 3.0 – hence the analyses are regarded as reliable in terms of oxide proportions. Compositional differences between the sphenes occurring in barroisitic amphibolites versus the analyzed sphene from a prasinite are not apparent from the data of Table 9.

Table 9. *Electron microprobe analyses of sphenes from eclogitic rocks, Gruppo di Voltri, Ligurian Alps*

Oxide	Sample number EE-12 hb	EE-72 hb	EE-95
SiO_2	30.81	30.77	31.34
Al_2O_3	0.84	1.52	2.47
TiO_2	36.36	40.95	39.22
FeO	0.36	0.42	0.34
Cr_2O_3	0.02	0.00	0.02
MgO	0.01	0.00	0.00
MnO	0.02	0.00	0.01
CaO	27.21	27.60	27.77
Na_2O	0.02	0.04	0.03
K_2O	0.00	0 00	0.01
Total	95.65	101.30	101.21

GRAPHIC ANALYSIS

Chemographic treatment of the eclogitic paragenesis developed in metagabbroic rocks of the Beigua serpentinite is difficult owing to a minimal number of chemical constraints in this system. As evident from the last two sections, approximately 10–13 components are required to characterize the compositional variations of the minerals, but individual stable assemblages consist of many fewer phases – on the order of three to six. For this reason, simplifying assumptions must be made which severely limit the utility of any graphical analysis. Nevertheless, as an aid in elucidating the overall reactions relating the several assemblages, a chemographic analysis similar to that previously presented for low-grade metabasaltic rocks will be employed (ERNST, 1963).

We recognize the importance of the following components: SiO_2; Al_2O_3; TiO_2; Fe_2O_3; FeO; MnO; MgO; CaO; Na_2O, K_2O, P_2O_5, S and H_2O. Some of these constituents are of consequence in only a few of the specimens and, where present, merely result in the appearance of an additional, indifferent phase; for instance, phosphorus, potassium and sulfur stabilize the accessories apatite, phengite and pyrite, respectively. More important is titanium, which invariably occurs in amounts exceeding that required for the Ti-saturation of the major rock-forming minerals; hence rutile appears in stages A and B and part of stage C, sphene becomes stable in stages C–E. Strictly speaking, these are not indifferent phases inasmuch as one or more of the major silicates must be involved in the conversion of rutile to sphene; however, the paragenesis is obscure and will not be treated here. Although quartz is never abundant in these metabasaltic rocks, it does occur sporadically in assemblages of all five stages, hence SiO_2 may be conveniently regarded as an excess component. In the eclogitic

rocks, the chemical potential of H_2O could have been low, whereas in the amphibole- and chlorite-bearing later stages C–E, μ_{H_2O} probably approached a value appropriate to this constituent in an aqueous fluid phase – as has been inferred for similar eclogite → amphibolite parageneses in other parts of the Alps (FRY and FYFE, 1971); here we provisionally assume H_2O-deficient conditions in the eclogitic stages, H_2O-excess conditions in the later stages. For the range of phase compositions analyzed in this investigation, Fe^{2+} + Mg (+ Mn) seem to be mutually exchangeable, so for graphic treatment of the phase assemblages we are justified in combining them as $R^{2+}O$; likewise, Al and Fe^{3+} are more or less interchangeable, hence may be lumped as $R_2^{3+}O_3$.

We are thus left with four determining constituents, Ca, Na, R^{2+} and R^{3+} (or their oxide equivalents). The chemical variables combined as R^{2+} and as R^{3+} will be distinguished and treated in the next section, which deals with element fractionation between coexisting phases. Equilibrium assemblages to be studied graphically therefore consist of up to four critical minerals plus a Ti-bearing phase, and perhaps accompanied by one or more accessories such as quartz, phengite, apatite, pyrite and aqueous fluid. To the extent that the assumptions are invalid, additional stable phases could be present, but in general the petrographic relationships do not suggest that this is so.

Figure 14 presents the simplified chemographic analysis of eclogitic parageneses in the Gruppo di Voltri in terms of Ca, Na, R^{2+} and R^{3+}. Only minerals observed and chemically analyzed in the present electron microprobe study are shown, hence the diagrams are incomplete; if valid, they apply strictly only to iron-rich basaltic bulk compositions such as those which characterize the metagabbroic rocks of the Beigua serpentinite (MOTTANA and BOCCHIO, 1975; CORTESOGNO et al., in press).

Clearly the eclogitic assemblages of stages A and B are situated within a high variancy phase field, with late garnet and Na-clinopyroxene systematically enriched in R^{2+} and in NaR^{3+}, respectively, compared to the premylonitic growth phases. Conversion to glaucophanic "eclogites" of stage C involved first, the stabilization of sodic amphibole relative to Na-clinopyroxene for these iron-rich bulk compositions, then the replacement of the garnet-omphacite tie line by the three-phase triangle glaucophane-epidote-barroisitic hornblende. Obviously H_2O was consumed during both of these reactions. The typical metabasaltic product assemblage tetrahedron is shown in Fig. 14, namely glaucophane + epidote + barroisitic hornblende + garnet rim. At some point within stage C, omphacite itself must have reacted with aqueous fluid to produce chiefly sodic amphibole, epidote and albite, but this has been omitted for simplicity. Next, but likewise not illustrated, the remaining garnet was replaced principally by the more hydrous compatibility chlorite + minor epidote. Stage C terminated through the replacement of the tie line linking Na-clinoamphibole with epidote by the three-phase triangle albite-hornblende-chlorite. Accordingly, stage D

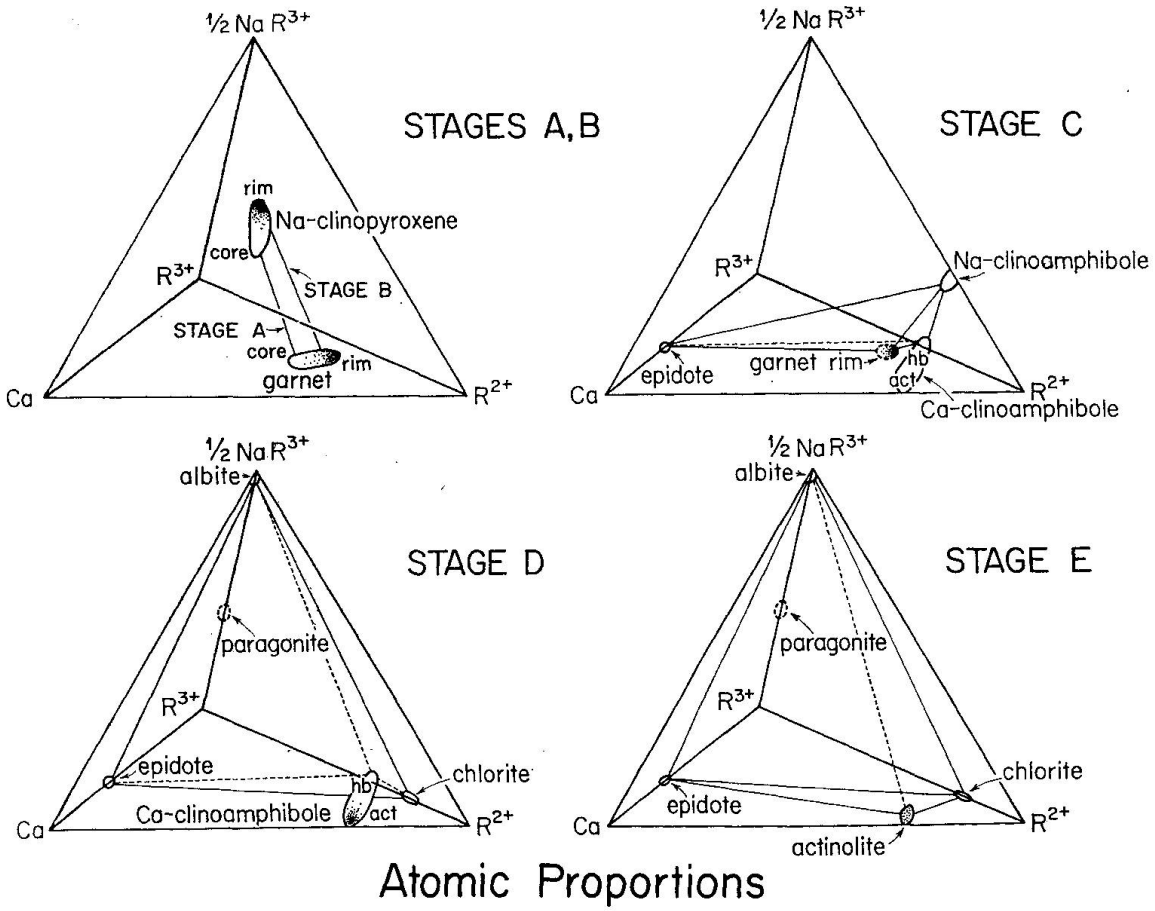

Fig. 14. Assemblage tetrahedra for eclogitic parageneses developed in iron-rich mafic rocks of the Beigua serpentinite, Gruppo di Voltri. Three apexes of the tetrahedron lie in the plane of the paper: $Ca-0.5NaR^{3+}-R^{2+}$ ($R^{3+}=Al+Fe^{3+}$; $R^{2+}=Mg+Mn+Fe^{2+}$). The fourth apex, R^{3+}, is shown directed oliquely towards the reader. Garnet lies on the front face $Ca-R^{3+}-R^{2+}$, omphacite lies on the lower face $Ca-0.5NaR^{3+}-R^{2+}$, and the clinoamphiboles lie close to the same basal face. Rutile is characteristic of stages A and B$\pm$C, sphene of stages C–E; The presence of an aqueous fluid is postulated in the later metamorphic stages but not in the eclogitic stages. Additional accessory phases such as quartz, phengite, apatite or pyrite may be present in specific assemblages, depending on the parental rock bulk composition.

assemblages consist of barroisitic amphibole, epidote, chlorite and albite. Small amounts of H_2O were consumed during this transformation too. The conversion of albite amphibolites to the typical prasinitic assemblage of stage E reflects the gradual recrystallization of the Na + Al-rich calcic amphibole to a more actinolitic composition as it diminished in amount, and by a comensurate increment in the proportions of albite, epidote and chlorite. In both stages D and E, the occurrence of more aluminous bulk compositions would have favored the assemblage paragonite + albite + chlorite + epidote – evidently the case in several of the investigated schists.

Although the compositions of the participating minerals have been elucidated in this study, univariant, stoichiometrically balanced reactions have not been attempted because the equilibria are certainly multivariant. Therefore, these

transformations must take place over broad zones in P-T-x space, with the compositions and proportions of the reactant and product minerals changing continuously with physical conditions. Nevertheless, the approximate nature of the join shifts is adequately illustrated in Fig. 14. It is evident from this figure that the paragenetic sequence A → E involves a systematic change in the chemical range of solid solution among clinopyroxenes, Na- and Ca-clinoamphiboles and garnets. As will be discussed further on (see Fig. 21), this phenomenon reflects first an apparent increase in the ratio P/T passing from stage A to B, then a decline in temperature or an increase in μ_{H_2O} during the middle stages of the metamorphism, and towards the end, a marked decrease in total pressure as well. The progressive change in Fe^{3+}/Al ratio of the epidote group minerals with grade (which cannot be represented in Fig. 14) also is compatible with an overall decrease in temperature during the later stages of recrystallization. The higher degree of hydration of the late assemblages may reflect this inferred thermal history, or it could be due to the increasing availability of an aqueous fluid phase during stages C–E, under nearly isothermal conditions.

ELEMENT PARTITIONING

Theory

The phenomenon of element fractionation between coexisting minerals was systematically treated first by RAMBERG and DEVORE (1951); the subject has since been investigated in considerable detail by numerous workers (e.g., see the synthesis and references cited by SAXENA, 1973). In principle, the disproportionation of elements between specific phases is examined as a function of mineral compositional ranges, it being assumed that all assemblages formed in equilibrium under a common set of physical conditions. The fundamental relationship for the over-all partitioning is that given by the Van't Hoff reaction isotherm,

$$\Delta G = \Delta G^\circ + RT \ln \frac{a_L^l \, a_M^m}{a_A^a \, a_B^b}, \tag{1}$$

for a heterogeneous equilibrium of the sort $aA + bB = lL + mM$. Here ΔG and ΔG° are the Gibbs free energy change and the standard state Gibbs free energy change of the reaction; A, B, L, and M represent the individual species involved in an exchange equilibrium involving two solid solutions; and a, b, l, and m are the stoichiometric coefficients of the reaction. A typical partition reaction involves the exchange of two components between a pair of phases, and may be indicated more simply as $lA_I + mB_{II} = lB_I + mA_{II}$, where A and B refer to

the discrete chemical species involved, l and m indicate the moles of ions being exchanged, and I and II represent the two coexisting phases. To begin with, we have ignored the possibility that either or both of the participating phases contain structurally distinct sites which can accommodate the exchangeable ions. Dividing by l, and letting m/l = n, our exchange equilibrium may be written as $A_I + n B_{II} = B_I + n A_{II}$. This reaction is related to the Gibbs free energy change by means of the Van't Hoff reaction isotherm as just presented:

$$\Delta G = \Delta G^\circ + RT \ln \frac{(a_B)_I (a_A)^n_{II}}{(a_A)_I (a_B)^n_{II}}, \tag{2}$$

or, on rearranging,

$$\Delta G = \Delta G^\circ + RT \ln (a_B/a_A)_I (a_A/a_B)^n_{II}, \tag{3}$$

where the activity of A in phase I is designated $(a_A)_I$. At equilibrium, the Gibbs free energy change of the reaction is zero, and expression (3) reduces to

$$-\Delta G^\circ = RT \ln (a_B/a_A)_I (a_A/a_B)^n_{II}. \tag{4}$$

Assuming that the activity coefficients are of unit value (i.e., ideal solution behavior), we can replace the activities by mole fractions or concentrations of the ions, X_A and X_B. The advantage here is that mole fractions and concentrations are readily measurable properties whereas, for our complex chemical system (especially clinoamphiboles and clinopyroxenes), the activities are not easily or unambiguously obtained. The distribution constant, K_D, may be defined in terms of the standard Gibbs free energy change of the partition reaction (at the T and P of interest)

$$e^{-\Delta G^\circ/RT} = K_D = (X_B/X_A)_I (X_A/X_B)^n_{II}. \tag{5}$$

Where component B approaches infinite dilution, $(X_A)_I \approx (X_A)_{II} \approx 1.0$ and the above expression reduces to

$$K_{ND} = (X_B)_I / (X_B)_{II}, \tag{6}$$

a statement of the Nernst distribution law (this relationship assumes that there is no coupling between trace and major constituents). The exponent n has unit value in dilute solutions provided the exchange is ion-for-ion.

Differentiating equation (5) with respect to temperature and pressure yields

$$(\partial \ln K_D/T)_P = \Delta H^\circ/RT^2, \tag{7}$$

or, rearranged,

$$\left(\frac{\partial \ln K_D}{\partial (1/T)}\right)_P = -\Delta H^\circ/R, \tag{8}$$

where ΔH° is the enthalpy change of the reaction, and

$$(\partial \ln K_D/\partial P)_T = -\Delta V^\circ/RT, \tag{9}$$

where $\Delta V°$ is the volume change of the reaction. It is apparent from equations (7) and (8) that, unless the enthalpy change is strongly dependent on the temperature, variation of the distribution constant with temperature should be less pronounced at elevated temperatures than at lower temperatures. More importantly, as is seen from equation (5), K_D will more closely approach unit value at high temperatures unless the absolute change of $-\Delta G°$ is proportional to the increment in temperature. Change in total pressure usually does not affect K_D as significantly, because volume changes in exchange reactions are generally small (see equation 9). By rearranging the terms of equation (5) we obtain the expression

$$K_D(X_B/X_A)^n_{II} = (X_B/X_A)_I. \tag{10}$$

This equation defines a straight line on a log-log graphical plot of $(X_B/X_A)_I$ on the ordinate versus $(X_B/X_A)_{II}$ on the abscissa, provided that the values of K_D and n are not a function of composition of either phase I or phase II. Where $(X_B/X_A)_{II}$ is unity, the horizontal intercept on the ordinate indicates the numerical value of K_D; the slope of the line gives the value of n (an ion-for-ion type of exchange would be revealed by a 45° slope).

As first pointed out by MUELLER (1962), because structurally complex silicates possess a variety of sites which accommodate the exchangeable cations, values of K_D are a composite function of the sublattice distributions, which in turn depend on order-disorder relations. This subject has been explored in detail for relatively "simple" minerals such as olivines, orthopyroxenes and binary feldspars by MATSUI and BANNO (1965), MUELLER (1969), THOMPSON (1969), and GROVER and ORVILLE (1969). Unfortunately, the important rock-forming minerals analyzed from the Gruppo di Voltri eclogitic parageneses include compositionally intermediate clinopyroxene, clinoamphibole and garnet solid solutions, all of which are crystallochemically extremely complex. In addition to this problem, treatment of the element partitioning among these coexisting phases is hampered by the lack of ferrous-ferric analytical data and hydroxyl concentrations. For these reasons, insofar as possible, we will make the simplest assumption by treating the exchange equilibria as ideal, ion-for-ion, and involving essentially single site minerals. Departure of the measured element fractionations from ideal distribution curves then may be regarded as a measure of the inapplicability of the assumptions and/or the failure of the phases to maintain chemical equilibrium with each other during crystallization.

Major element distribution

(See equation 10.) First let us consider the fractionation of ferrous iron and magnesium between various mafic minerals from the Voltri complex. Remem-

ber that for garnets, Ca clinoamphiboles and chlorites, all the iron has been regarded as divalent, whereas for the purpose of calculation, ferrous-ferric ratios of unit value have been assigned to sodic amphiboles and omphacites. In the section dealing with mineral compositions it was shown that for the sodic clinopyroxenes this assumption appears to be valid, whereas glaucophanes probably tend to be slightly richer in Fe^{2+} than in Fe^{3+}. Figure 15 illustrates the disproportionation of ferrous iron and magnesium between the coexisting pairs: (a) garnet + clinopyroxene; b) garnet + sodic amphibole; (c) calcic amphibole + sodic amphibole; and (d) calcic amphibole + chlorite. In all examples, 45° partition curves have been visually estimated and added for reference only.

In Fig. 15a, it is apparent that stage A clinopyroxene + garnet cores exhibit a pronounced Fe^{2+}/Mg partitioning, with a K_D value approaching 30. Understandably, the eightfold coordinated structural site of garnet strongly concentrates ferrous iron relative to the much smaller sixfold coordinated site of clinopyroxene. The marked scatter of iron-magnesium ratios for garnet rims + stage B omphacites probably is a consequence of the fact that garnets continued growth after the Na clinopyroxenes began to be replaced by glaucophane (see Fig. 3); hence in this case we may not be dealing with a stable analyzed assemblage, but instead with the persistence of partly replaced relict clinopyroxenes with early stage C garnets. The association of sodic amphibole with all nine post-stage A garnet + omphacite pairs shown in Fig. 15a supports this explanation.

A somewhat similar argument may be advanced to account for the garnet rim + glaucophane ferrous iron-magnesium distribution illustrated in Fig. 15b. Both Fe^{2+} and Mg increased during the period of garnet growth and, although the mole fraction of Alm thereby increased, it did so at a much lesser rate than the increment in Py – consequently the analyzed ferrous iron-magnesium ratio of the garnets decreases towards the rim (see also Fig. 4). Inasmuch as the sodic amphiboles have replaced the earlier omphacites, their Fe^{2+}/Mg ratios could conceivably simply mirror the compositions of the pre-existing chain silicates. On the other hand, if the sodic amphibole from sample EE-63 is ignored (it can be seen from Table 3 that this glaucophane contains a rather high CaO content, but otherwise appears to be comparable to the other analyzed sodic amphiboles), the remaining nine more or less lie along a partition curve possessing a K_D value of about 28. The concentration of magnesium ions in the small octahedral sites of the Na clinoamphibole relative to the large eightfold structural site of garnet seems quite reasonable.

The partitioning of Fe^{2+} and Mg between hornblende or actinolite and sodic amphibole is shown in Fig. 15c. It is unclear why ferrous iron should be concentrated preferentially in barroisitic hornblende relative to sodic amphibole ($K_D = 3.0$) and why the Fe^{2+}/Mg distribution should be sensibly the same in actinolite + glaucophane pairs ($K_D = 1.0$). Judging from the textural relations

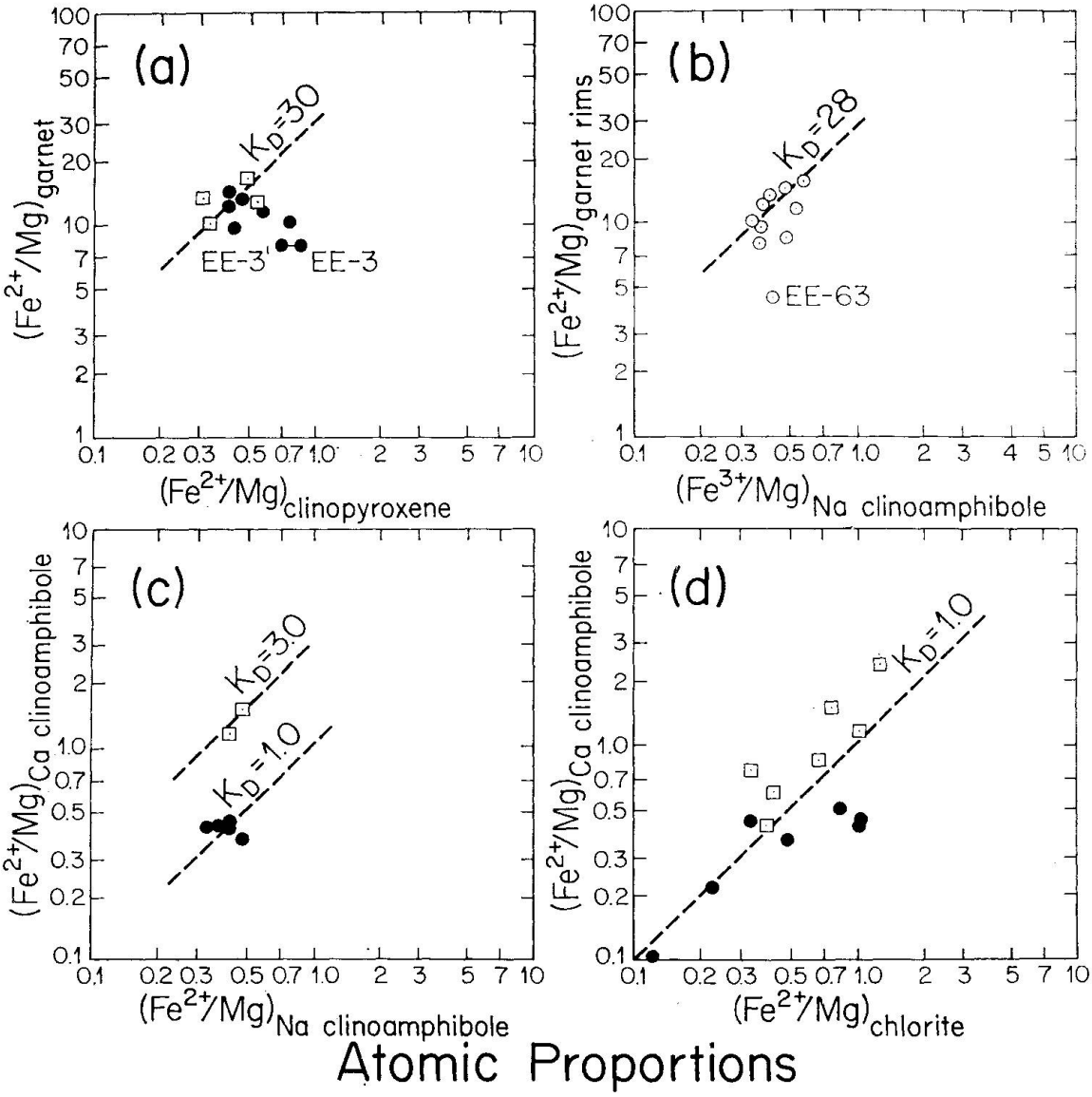

Fig. 15. Ferrous iron-magnesium partitioning between coexisting pairs of mafic silicates from the Gruppo di Voltri eclogitic lenses. In (a) open squares represent compositions of garnet cores + clinopyroxenes of stage A, filled circles garnet rims + stage B clinopyroxenes; pairs of clinopyroxene analyses (Table 2) are presented to provide an estimation of the reproducibility of the data. The Fe^{2+}/Mg ratios of associated garnet rims + sodic amphiboles are shown in (b). In (c) and (d), squares indicate the coexistence of barroisitic hornblende with sodic amphibole and chlorite, respectively; filled circles refer to more actinolitic calcic amphiboles.

described in the section dealing with mineral paragenesis (see also Fig. 3), actinolite + glaucophane does not represent an equilibrium association in the Voltri eclogitic paragenesis, hence possibly the replacing Ca clinoamphibole merely acquired its bulk Fe^{2+}/Mg ratio from the glaucophanic growth substrate. In the case of the two barroisite + sodic amphibole pairs, it seems likely from Fig. 7b that the blue amphibole contains more ferrous and less ferric iron than has been

assumed, whereas the probable presence of any trivalent iron in the hornblende would lower its ferrous content; therefore, the K_D value of 3.0 undoubtedly represents a maximum for such equilibrium pairs.

The distribution of Fe^{2+} and Mg in calcic amphiboles and associated chlorites are shown in Fig. 15d. Taking the group as a whole, there is no obvious concentration of either ferrous iron or magnesium in calcic amphibole with respect to chlorite. However, barroisites display a systematic but slight enrichment in Fe^{2+}/Mg ratio relative to chlorite, whereas actinolitic amphiboles tend to be a little more magnesian than the coexisting chlorites.

Only one epidote + sodic amphibole pair was analyzed in this study, so to consider ferric iron-aluminum fractionation we are obliged to confine our attention to epidote + plagioclase assemblages. The Fe^{3+}/Al partitioning and a visually estimated distribution curve are presented in Fig. 16. Clearly, as indicated by a K_D value of 50, epidote strongly concentrates ferric iron relative to the sodic plagioclase. This is a consequence of the large octahedral site available in epidote, compared to the exclusively small four-fold coordinated cation position of the feldspar structure. As is also clear, barroisitic amphibolites are characterized by relatively Fe^{3+}-rich epidote and plagioclase, whereas the ferric iron contents of these phases are correspondingly reduced in the actinolitic greenschists.

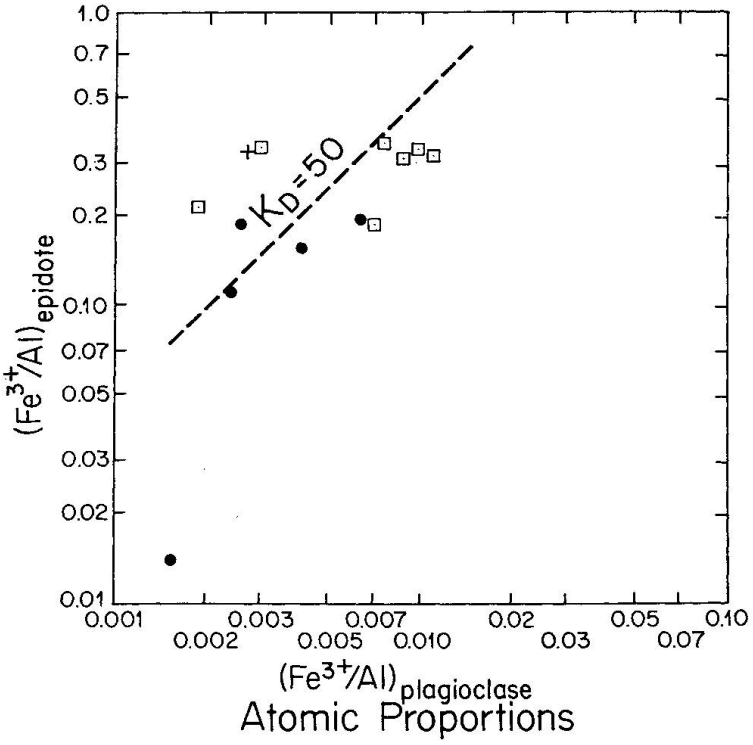

Fig. 16. Ferric iron-aluminum partitioning between coexisting pairs of epidote + plagioclase from the Voltri Massif. Open squares represent assemblages containing barroisitic hornblende, filled circles indicate actinolite-bearing assemblages.

Minor element distribution

(See equation 6.) Partitionings of the minor elements titanium and manganese between the coexisting mafic pairs (a) garnet + clinopyroxene, (b) garnet + sodic amphibole, (c) calcic amphibole + sodic amphibole, and (d) calcic amphibole + chlorite are shown in Figs. 17 and 18, respectively. Values are given in terms of oxide weight percents rather than in cation mole proportions as in Figs. 15 and 16, but as is clear from equation (6), the evaluation of K_{ND} is independent of the manner of minor element presentation (e.g., as titanium or manganese ion, oxide, or silicate "end member" proportions; this is so because the entire matrix for both phases is proportional to the element concentration, hence cancels out of the expression leaving the Nernst infinite dilution distribution constant in terms of the Ti or Mn ratio.

As may be seen from Fig. 17, earlier, higher grade minerals in general – and garnet cores and barroisitic hornblendes in particular – contain more titanium than do the subsequent, lower grade phases. However, the disproportionation of Ti between coexisting minerals is thoroughly obscured by the tendency for chain silicates, especially the stage A omphacites and, to a lesser extent the barroisites, to exsolve a Ti-bearing oxide phase during later portions of the recrystallization event (see petrographic descriptions in section dealing with the mineral paragenesis). For this reason it is difficult to draw firm conclusions from the fractionation data of Fig. 17. Distribution curves for $K_{ND} = 1$ have been added only as an aid to show the reader the extent of disproportionation and systematics – if any. Several observations can be made however. (1) Garnet cores possess higher Ti contents than their rims, whereas there is no obvious difference in the titanium contents of clinopyroxenes from stage A versus stage B (Fig. 17a). This probably means that all omphacites have to some extent exsolved titanium during lower grade annealing. (2) Sodic amphiboles are uniformly low in Ti compared to both garnet rims and barroisite (Figs. 17b and c, respectively). (3) Hornblendes carry more titanium than do actinolites, but all calcic amphiboles are strongly enriched in this element compared to coexisting chlorite (Fig. 17d).

In contrast to titanium, the manganese fractionation tends to be considerably more systematic in the analyzed mafic mineral pairs. This is probably a consequence of the fact that Mn is retained by the phases during later stages of the recrystallization rather than forming separate exsolution lamellae in the host silicates. As was discussed in the section on mineral chemistry, Mn concentrations in garnet cores exceed minor element values. Nevertheless, the distribution of this element between garnet + clinopyroxene and between garnet + sodic amphibole pairs (Figs. 18a and b, respectively) appears to obey the infinite dilution law, with Mn strongly concentrated in the garnet relative to the chain silicates. Calcic amphiboles also seem to be markedly enriched in

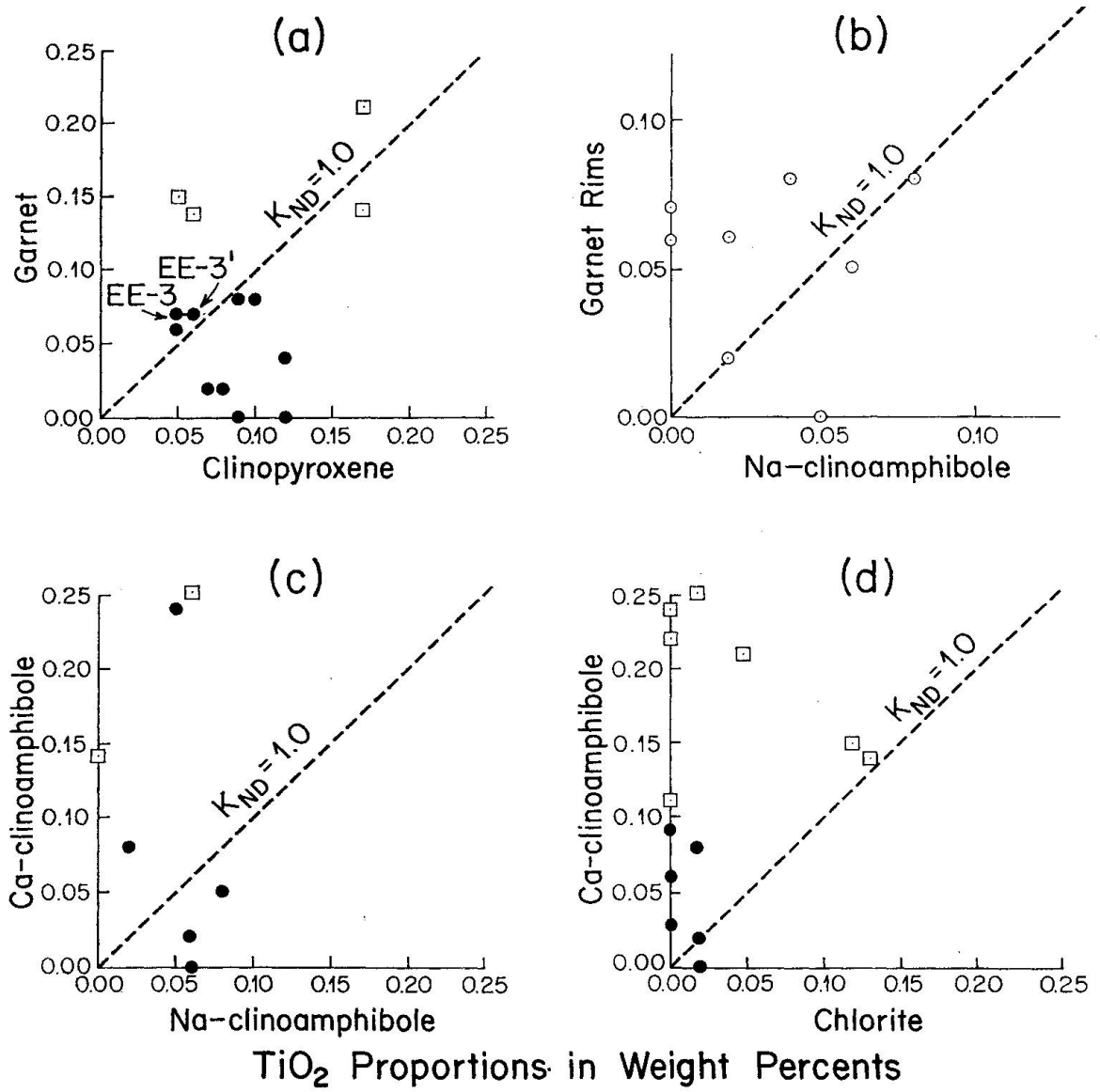

Fig. 17. Titanium fractionation between coexisting pairs of mafic silicates from the Gruppo di Voltri eclogitic lenses. Symbols correspond to those of Fig. 15.

manganese relative to coexisting sodic amphiboles, but the five data points representing actinolite + glaucophane pairs presented in Fig. 18c should be discounted inasmuch as these phases are not regarded as an equilibrium association in the Ligurian eclogitic paragenesis. Figure 18 demonstrates that there is a more or less equal distribution of Mn between calcic amphiboles and coexisting chlorites.

Before leaving the subject of minor elements, let us briefly consider the disproportionation of chromium between analyzed mafic silicate pairs. The 83 bulk rock analyses presented by CORTESOGNO et al. (in press) average about 130 ppm Cr. Consequently, the chromium contents of the constituent minerals in the

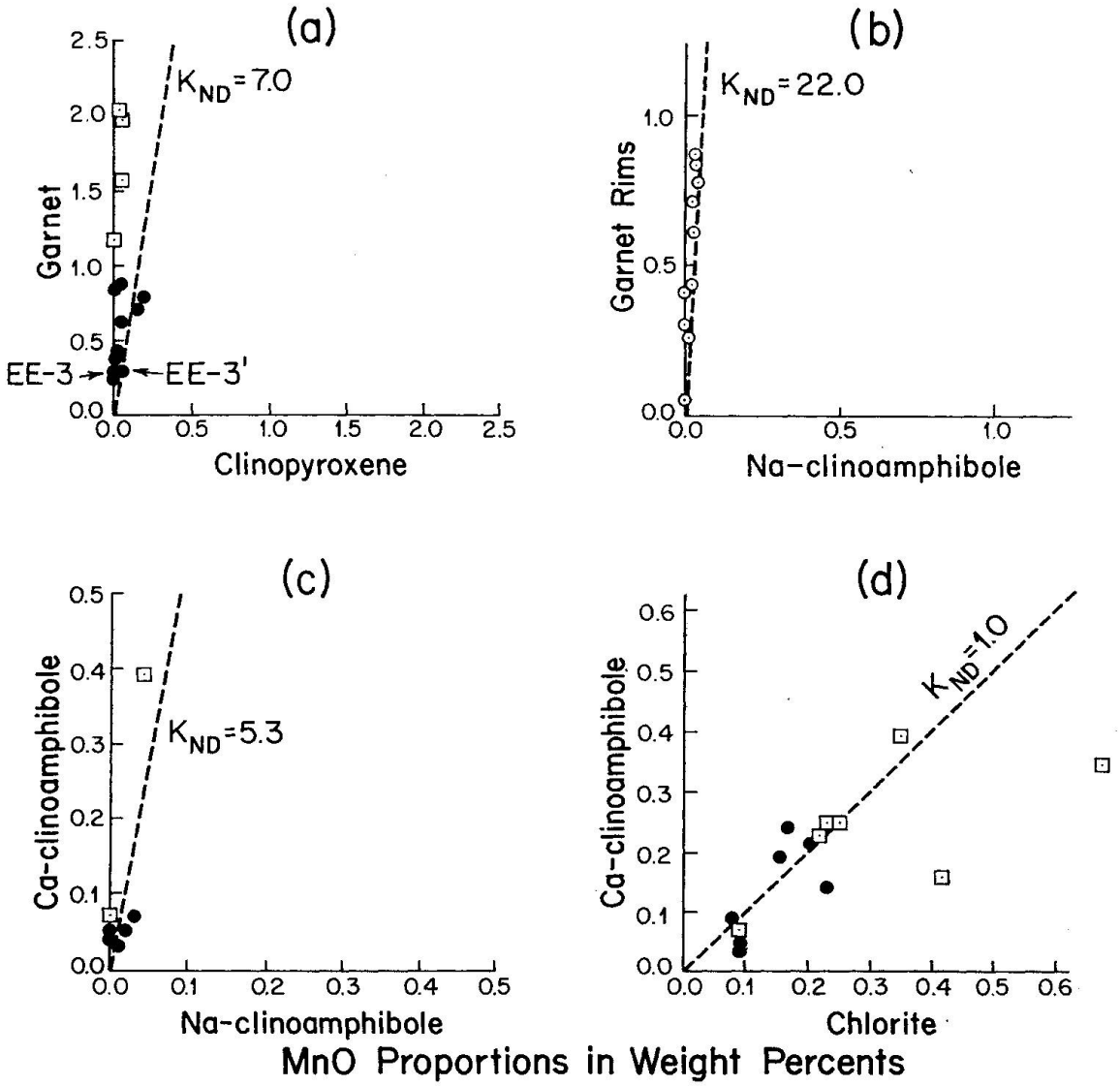

Fig. 18. Manganese fractionation between coexisting pairs of mafic silicates from the Gruppo di Voltri eclogitic lenses. Symbols correspond to those of Fig. 15.

Voltri complex are so low that the amounts are approximately at the detection limit. Of the 25 rocks for which microprobe analyses of the coexisting minerals were obtained in the present study, only sample EE-12 lacks a whole rock XRF analysis. Of the 24 for which bulk chemistry is available, high Cr contents are reported by CORTESOGNO et al. for the following: EE-17 = 260 ppm; EE-24 = 215 ppm; EE-64 and EE-74 = 350 ppm. The Cr_2O_3 contents for the analyzed minerals from these four rocks are listed in Table 10; it should be noted that opaque phases, which probably contain appreciable chromium were not analyzed in the electron microprobe investigation – hence these phases are not tabulated. Although few data are available, in general it appears that early-formed omphacite (stage A clinopyroxene) and early barroisitic hornblende

Table 10. *Cr_2O_3 contents of analyzed minerals from relatively chrome-rich rocks in weight percent*

Mineral	Sample number EE-17 prasinite	EE-24 prasinite	EE-64 eclogite	EE-74 eclogite
Garnet core	–	–	0.00	–
Garnet rim	–	–	0.00	–
Clinopyroxene A	0.83	–	–	–
Clinopyroxene B	–	–	0.00	–
Sodic amphibole	–	–	0.03	–
Hornblende	–	0.48	–	–
Actinolite	0.08	–	–	0.02
Epidote	0.00	0.16	–	0.03
Chlorite	0.40	0.00	–	0.04
Sodic plagioclase	0.00	0.02	–	0.00
Phengite	–	–	–	0.12

concentrated the Cr, whereas this element was rejected by garnet, sodic amphibole and plagioclase. Chlorite, potassic white mica, epidote and actinolite seem to have incorporated variable but intermediate amounts of chromium compared to the other analyzed phases.

PETROLOGIC DISCUSSION

Documentation of the crystallochemical evolution of phase assemblages in the eclogitic lenses of the Gruppo di Voltri presented in previous sections inevitably leads to the question of genesis. Based on the great density of eclogitic rocks as well as their petrologic occurrences, ESKOLA (1914, 1939) recognized their relatively high-pressure origin and considered them as representatives of a specific metamorphic mineral facies. Although COLEMAN and others (1965) questioned the usefulness of the concept of an eclogite facies, they pointed out that such rocks may be divided into three distinct groups based on contrasting mode of occurrence and mineral chemistry; their lowest grade category, group C eclogites, which are found associated with glaucophane schists and as lenses in alpine-type peridotites, are characterized by pyrope-poor garnets (Py < 30 mole percent) and jade-rich omphacites (Jd > 30 mole percent). Clearly the eclogites included in the Beigua serpentinite belong to group C, both in terms of mineral chemistry and lithologic association. The partitioning of ferrous iron and magnesium between garnet + clinopyroxene pairs was investigated for various eclogitic masses in the Franciscan and Sanbagawa belts and compared with other occurrences by ERNST et al. (1970, Chapter IX) and by BANNO (1970); these authors showed that for California (type C) eclogites, K_D values cluster around 20–23 – reasonably close to the K_D value of 30 reported in the present paper for garnet core + stage A omphacites from the Voltri eclogites.

(Note also that lower K_D values would appear to be appropriate for post-mylonitic garnet rims + stage B clinopyroxene pairs as seen from Fig. 15; as previously mentioned, however, this does not appear to represent an equilibrium assemblage.) We may conclude from these petrologic and chemical studies that the eclogitic rocks investigated in this report crystallized at moderate temperatures and relatively high pressures, similar to other type C occurrences.

Experimental phase equilibrium investigations of the basalt-eclogite transformation have been conducted by many different workers (YODER and TILLEY, 1962; RINGWOOD and GREEN, 1966; GREEN and RINGWOOD, 1967; COHEN et al., 1967; LAMBERT and WYLLIE, 1972). The data are compatible at near solidus temperatures, but extrapolated phase boundaries diverge at lower temperatures. The exact nature, width and location of the plagioclase eclogite + garnet granulite transition zone around 300–700° C is still a matter of discussion, largely because the experimental transformations have not been produced due to sluggishness of the reactions at such low temperatures. Nevertheless, it is clear that eclogitic assemblages represent the high-pressure anhydrous equivalents of metabasaltic granulites and pyroxene hornfelses. At moderate and high values of μ_{H_2O}, such assemblages are replaced by amphibolitic phase compatibilities (YODER and TILLEY, 1962; ESSENE et al., 1970; LAMBERT and WYLLIE, 1972). As demonstrated by GREEN and RINGWOOD (1967, Fig. 7), mafic bulk compositions characterized by a high Fe^{2+}/Mg ratio – such as those typical of the Voltri rocks – develop garnet at lower pressures than do more magnesian bulk compositions. However, their investigations also showed that metabasaltic bulk compositions higher in alkalis (and silica) favored the stabilization of plagioclase to greater pressures compared with CaO + MgO-rich whole rock compositions. Therefore, at low values of μ_{H_2O}, the FeO + Na_2O-rich metabasaltic rocks of the Gruppo di Voltri would be expected to display a very broad garnet granulite transition zone situated between the P-T fields characterized by high-pressure eclogitic and low-pressure mafic granulitic phase assemblages.

In an attempt to estimate the physical conditions of origin for the Ligurian eclogitic paragenesis, let us return to a consideration of ferrous iron and magnesium disproportionation between garnet and clinopyroxene. The exchange equilibrium for this element partitioning may be written as

$$\underset{\text{Py}}{\tfrac{1}{3}Mg_3Al_2Si_3O_{12}} + \underset{\text{Hd}}{CaFe^{2+}Si_2O_6} = \underset{\text{Alm}}{\tfrac{1}{3}Fe^{2+}_3Al_2Si_3O_{12}} + \underset{\text{Di}}{CaMgSi_2O_6}$$

or, more simply

$$(Mg)_{\text{garnet}} + (Fe^{2+})_{\text{clinopyroxene}} = (Fe^{2+})_{\text{garnet}} + (Mg)_{\text{clinopyroxene}}.$$

If thermochemical data were available for Py, Hd and Alm, the value of K_D as a function of T and P could be calculated employing equations (5), (8) and (9), but unfortunately this is not the case. The $\Delta V°$ of the reaction is reasonably

well known, hence using a value for ΔV° of -1.33 cm^3 for the exchange equilibrium as given above, BANNO (1970, Fig. 1) was able to evaluate the pressure coefficient of K_D; his computations involved the assumption of ideal solid solutions, negligible change of ΔV° as a function of state variables, and independence of K_D from bulk composition of the phases. Accepting BANNO's calculations (pressure coefficients for K_D are graphed in Fig. 20), the variation of the distribution constant with physical conditions may be determined if P and T for two or more independent equilibrium constants can be obtained.

BANNO (1970) showed that garnet + clinopyroxene pairs from type A, B and C eclogites possess K_D values averaging approximately 3.6, 9.1 and 23, respectively. MACGREGOR and CARTER (1970) suggested that type A eclogitic xenoliths from the Roberts Victor Mine, South Africa, crystallized under near-solidus conditions – hence employing the phase equilibrium studies referred to previously, we may provisionally assign minimum values for the conditions of genesis for these masses as 1300° C and roughly 25 kilobars. Type B eclogites' such as those from southern Norway (ESKOLA, 1921) are characteristic of high-rank amphibolite terranes representing deep crustal levels, hence appropriate values of T and P may be assumed to lie in the neighborhood of 700° C and 10 kilobars. Franciscan eclogites and type IV blueschists (COLEMAN and LEE, 1963) apparently crystallized at temperatures on the order of 500° C according to O^{18}/O^{16} measurements by TAYLOR and COLEMAN (1968); based on experimental phase equilibrium data, these authors argued persuasively for pressures of formation of about 10 kilobars.

Employing these approximate values, plus the pressure coefficient of K_D determined by BANNO (1970), the one atmosphere isobaric variation of the distribution constant with temperature can be evaluated, as shown in Fig. 19 (see also equation 8). Of course, at this pressure, the eclogite assemblage is metastable, but this fact does not invalidate the calculation. Rather surprisingly, and probably quite fortuitously, the data lie along a straight line, suggesting that in the range illustrated, ΔH° is sensibly independent of temperature, and the exchange reaction as written above evolves 5.8 kcal per mole of clinopyroxene. Again using BANNO's pressure coefficients, values of K_D as a function of the state variables may be plotted, as shown in Fig. 20. Evidently, if the premylonitic Voltri eclogites crystallized at a pressure on the order of 10 kilobars, the determined value for K_D of about 30 (see Fig. 15a) indicates a temperature of formation of approximately $440 \pm 50^\circ$ C.

RÅHEIM and GREEN (1974) have experimentally investigated the variation of iron-magnesium partitioning in coexisting garnet and clinopyroxene, and especially at low temperatures their K_D plot is very similar to that of Fig. 20. Again, assuming a 10 kilobar pressure of crystallization for the stage A eclogites of the Gruppo di Voltri, application of RÅHEIM and GREEN's experimentally obtained equation,

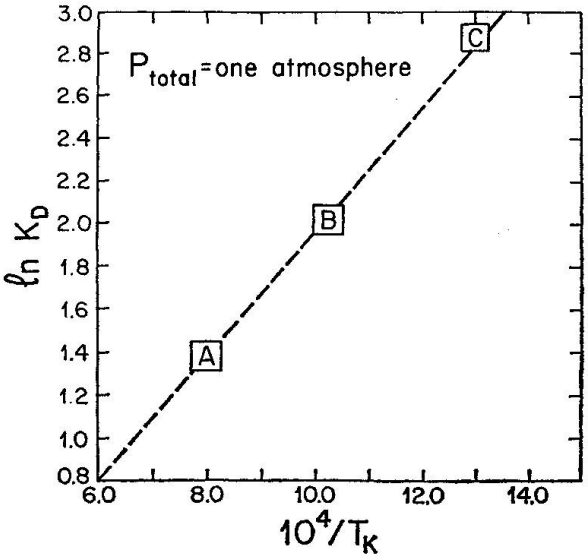

Fig. 19. One atmosphere isobaric plot of $\ln K_D$ versus $1/T_K$ for the fractionation of Fe^{2+} and Mg between coexisting garnet and clinopyroxene. Eclogite groups are: A = Roberts Victor Mine, South Africa; B = southern Norway; C = western California. K_D values are from BANNO (1970) corrected to one atmosphere total pressure. See text for discussion of assignment of operating state variables for these three eclogitic environments. The slope of the curve is $-\Delta H°/R$.

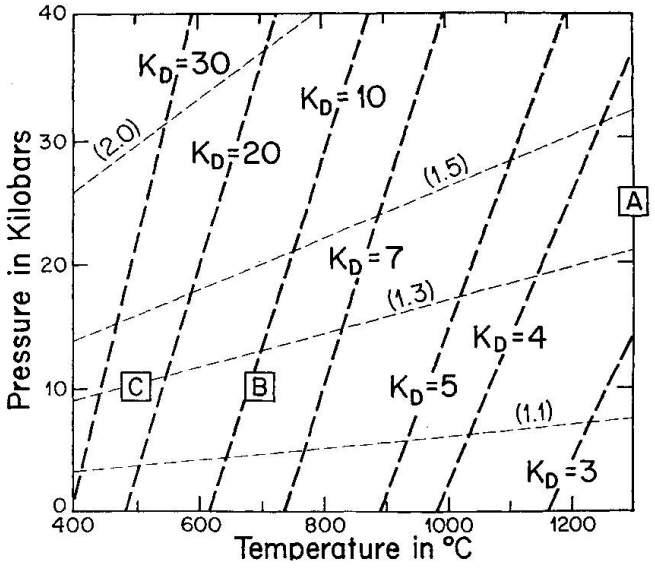

Fig. 20. Estimation of conditions of origin for eclogites from: Roberts Victor Mine, South Africa = A; southern Norway = B; western California = C. Pressure coefficients computed by BANNO (1970, Fig. 1) are shown as light dashed curves; the ratios of $(K_D)_P/(K_D)_0$ are indicated by parentheses. Employing the K_D values of A = 3.6, B = 9.1 and C = 23 and Fig. 19, the variation of K_D as a function of P and T is determined as shown by the heavy dashed lines.

$$T_K = \frac{3686 + 28.35\,P\ (\text{in kilobars})}{2.33 + \ln K_D},$$

yields a temperature of formation of 420° C. It therefore seems reasonable to accept provisionally a mean value of 430 ± 50° C as the temperature under which the early stage eclogitic assemblages were developed in the Voltri Massif. A figure of 10 kilobars is more difficult to substantiate, but a much lower confining pressure would place the assemblage within the plagioclase eclogite + garnet granulite transition zone (e.g., see ITO and KENNEDY, 1971).

COHEN et al. (1967) showed that, within the garnet granulite transition zone for mafic compositions, sodium is concentrated in plagioclase relative to clinopyroxene, and calcium in garnet relative to plagioclase. Thus, with isothermal increment in pressure, garnet would become less grossularitic, coexisting clino-

pyroxene more jadeitic, as the increasingly albitic plagioclase decreases in amount; such a conclusion may also be drawn from the subsolidus studies of various bulk compositions reported by GREEN and RINGWOOD (1967). However, once the eclogite field of stability is entered, the change in mineral compositions is likely to be less pronounced, but experimental data are not available regarding such chemical phase variations. It is known that the garnet/clinopyroxene ratio increases gradually with increasing pressure. Therefore, at a given temperature, higher-pressure eclogites would be expected to carry relatively Gross-poor garnets and Jd-rich clinopyroxenes compared to lower pressure equivalents. This is the situation for the eclogitic paragenesis in the Gruppo di Voltri, which suggests that, for the post-mylonitic eclogites, the Na-rich stage B omphacites and Ca-poor, Fe^{2+}-rich garnet rims attest to an increment in pressure. This discussion presumes an essentially isochemical recrystallization relating the eclogitic phase assemblages; it seems to be a reasonable hypothesis judging from the fact that CORTESOGNO et al. (in press) were unable to draw a bulk chemical distinction between stage A and stage B eclogites.

Blueschist assemblages typified by the association of glaucophane + garnet, later followed by the assemblage glaucophane + epidote + barroisite (+ albite) signalling the final decomposition of garnet, reflect stage C conditions. Judging from the similarity of these phase compatibilities with type IV glaucophane schists of California and New Caledonia – where oxygen isotope geothermometry investigations by TAYLOR and COLEMAN (1968) indicate temperatures exceeding those of type III blueschists (T = 285–315° C) – stage C blueschists of the Voltri eclogitic paragenesis probably recrystallized around 400° C, 8 kilobars. Presumably also the chemical potential of H_2O increased during this stage, as inferred from the generation of hydrous phases.

Passage of the assemblages through the amphibolitic stage D is poorly constrained in terms of physical conditions. Moreover, all that can be said confidently about the terminal prasinitization is that it began in upper greenschist facies P-T conditions, as indicated by the production of biotite, and terminated with lower greenschist facies assemblages (biotite unstable). Reasonably assigned state variables would seem to lie in the realm 300–375° C and 2–5 kilobars. The value of μ_{H_2O} probably was high, as reflected by the hydrous nature of the assemblages; probably a separate aqueous phase accompanied this recrystallization, judging by the apparent metasomatic effects reported for the prasinitic schists by CORTESOGNO et al. (in press).

Prograde and retrograde P-T trajectories are shown for the eclogitic rocks of the Beigua serpentinite in the petrogenetic grid of Fig. 21. The hypothetical prograde path follows an abnormally low geothermal gradient characteristic of subduction zone metamorphism (e.g., see ERNST, 1975); such a thermal regime apparently can be maintained only in a dynamic system where a relatively cool lithospheric plate (lithologic materials all possess low thermal conductivities)

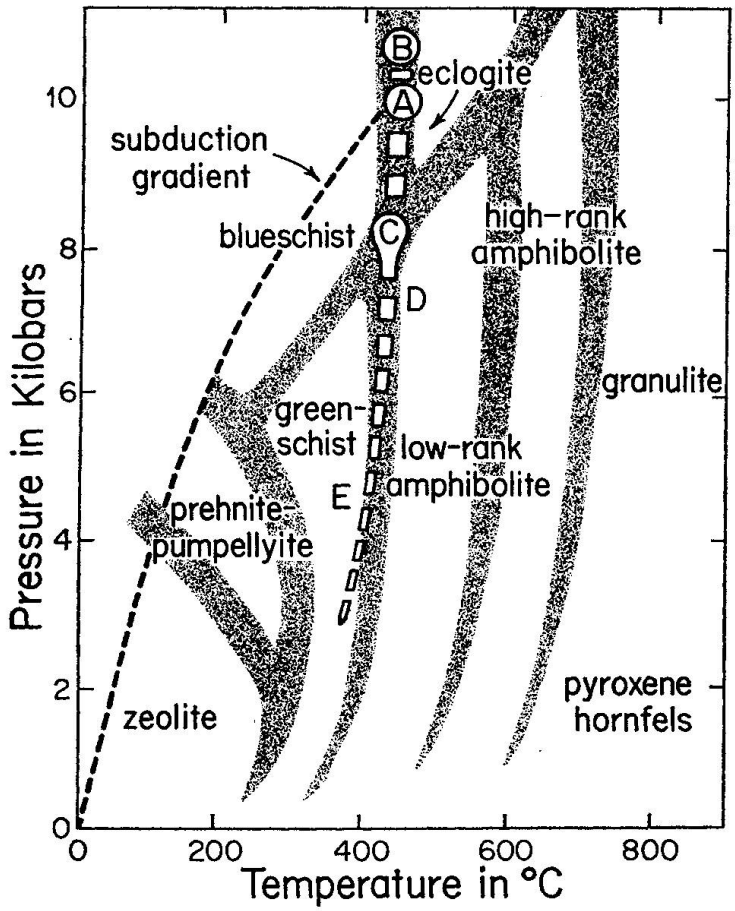

Fig. 21. Petrogenetic grid for a broad range of crustal rock compositions based on available experimental phase equilibrium and oxygen isotopic data, after ERNST (1973, Fig. 4). For simplicity, transition zones between pairs of metamorphic facies fields are illustrated using an arbitrary but minimal band width. The general prograde (subduction) and specific retrograde (buoyant uplift) P–T trajectories are shown for the eclogitic rocks of the Gruppo di Voltri. The dehydration of serpentine (not illustrated) lies at temperatures exceeding 500° C where aqueous fluid pressures are greater than a few hundred bars (BOWEN and TUTTLE, 1949; KITAHARA et al., 1966).

rapidly descends to great depths. The mechanism involving the postulated return of subducted and metamorphosed crustal rocks and the mantle underpinnings toward the surface is more difficult to understand (COLEMAN, 1972), but it evidently has taken place in Liguria and elsewhere in the Western Alps (ERNST, 1971; MARTINI, 1972; DAL PIAZ et al., 1972; DAL PIAZ, 1974a, b). CORTESOGNO et al. (in press) demonstrated that serpentinization of the Beigua peridotite occurred prior to the high-pressure metamorphism. And, as is apparent from Fig. 21, the entire recorded P-T history of the Beigua serpentinite and the enclosed eclogitic lenses evidently took place within the serpentine stability field (see BOWEN and TUTTLE, 1949; KITAHARA et al., 1966). Accordingly, decoupling and rise of this section of hydrated uppermost mantle fragment along an essentially adiabatic P-T path probably was driven at least in part by body forces in response to the buoyancy of the complex. Of course, convergent plate

margins such as the one recognized in Western Liguria are the site of strong compressional forces, so lateral tectonic transport undoubtedly played a role in the juxtaposition of these rocks with other sections described in the introduction.

It seems probable that the metamorphic mineral assemblages and deduced P-T trajectory documented in this paper and shown schematically in Figs. 3 and 21 reflect stages in the subduction and subsequent uplift of the Beigua serpentinite-eclogite complex. Probably stage A represents preculmination progressive subduction zone metamorphism in these rocks. The early deformation and post mylonitic growth of stage B clinopyroxenes and garnet margins may testify to a change in tectonic setting – and perhaps rapid loading – at the peak of the prograde metamorphism. The gradual access of aqueous fluids very likely accompanied decoupling of the studied units from the downgoing slab, with relatively rapid ascent towards the surface (unloading and slight cooling) manifest through the production of stages D and E barroisitic amphibolites and greenschists, respectively.

Acknowledgments

The research presented here represents part of a U.S.-Italy cooperative science project to investigate mafic and ultramafic rocks in Western Liguria. Support has been derived from the U.S. National Science Foundation (grant No. GA-37157X), the Italian Consiglio Nazionale delle Ricerche, the Università di Genova and the University of California, Los Angeles. In addition, the study was aided by the receipt of a Guggenheim Foundation Fellowship, which allowed me to undertake the electron microprobe study at the Eidgenössische Technische Hochschule, Zürich. I would like to thank all these institutions for support, and colleagues at Genova (L. Cortesogno, M. Galli, B. Messiga, G. M. Pedemonte and G. B. Piccardo), UCLA (Vicki Jones and Julie Knaack), and the ETHZ (W. Richter, J. Sommerauer and V. Trommsdorff) for help both in the field and the laboratory.

The manuscript has been reviewed and materially improved by S. Banno, Kanazawa University; L. Cortesogno, Università di Genova; I. D. MacGregor, University of California, Davis; and A. B. Thompson, Harvard University.

References cited

Banno, S. (1970): Classification of eclogites in terms of physical conditions of their origin. Phys. Earth and Planet. Interiors *3*, p. 405–431.

Bearth, P. (1959): Über Eklogite, Glaukophanschiefer und metamorphe Pillowlaven. Schweiz. mineral. petrogr. Mitt. *39*, p. 267–286.

— (1966): Zur mineralfaziellen Stellung der Glaukophan-Gesteine der Westalpen. Schweiz. mineral. petrogr. Mitt. *46*, p. 13–23.

— (1967): Die Ophiolithe der Zone von Zermatt–Saas Fee. Beitr. geol. Karte Schweiz, N.F. 132, 130 p.

— (1970): Zur Eklogitbildung in den Westalpen. Fortschr. Mineral. *47*, p. 27–33.

— (1971): Zum Chemismus der Eklogite und Glaukophanite von Zermatt. Schweiz. mineral. petrogr. Mitt. *51*, p. 349–359.

— (1973): Gesteins- und Mineralparagenesen aus den Ophiolithen von Zermatt. Schweiz. mineral. petrogr. Mitt. *53*, p. 299–334.

— (1974): Zur Gliederung und Metamorphose der Ophiolithe der Westalpen. Schweiz. mineral. petrogr. Mitt. *54*, p. 385–397.

Bocchio, R. e A. Mottana (1974): Le eclogiti anfiboliche in serpentina di Vara (Gruppo di Voltri). Rend. Soc. It. di Mineral. e Petrologia *30*, p. 855–891.

Bocquet, J. (1971): Cartes de répartition de quelques minéraux du métamorphisme alpin dans les Alpes franco-italiennes. Eclogae geol. Helv. *64*, p. 71–103.

Bowen, N. L. and O. F. Tuttle (1949): The system MgO-SiO_2-H_2O. Bull. Geol. Soc. America *60*, p. 439–460.

Chatterjee, N. D. (1971): Phase equilibria in the Alpine metamorphic rocks of the environs of the Dora-Maira Massif, western Italian Alps, Parts I and II. Neues Jahrb. mineral. Abh. *114*, p. 181–245.

Chiesa, S., L. Cortesogno, F. Forcella, M. Galli, B. Messiga, G. Pasquaré, G. M. Pedemonte, G. B. Piccardo e P. M. Rossi (1975): Assetto strutturale ed interpretazione geodinamica del Gruppo di Voltri. Boll. Soc. Geol. Italy *94*, p. 555–581.

Cohen, L. H., K. Ito and G. C. Kennedy (1967): Melting and phase relations in an anhydrous basalt to 40 kilobars. Am. Jour. Sci. *265*, p. 475–518.

Coleman, R. G. (1972): Blueschist metamorphism and plate tectonics. XXIV. Int. Geol. Congr., Montreal, Rept. Sec. 2, p. 19–26.

Coleman, R. G. and D. E. Lee (1963): Glaucophane-bearing metamorphic rock types of the Cazadero area, California. Jour. Petrology *4*, p. 260–301.

Coleman, R. G., D. E. Lee, L. B. Beatty and W. W. Brannock (1965): Eclogites and eclogites: their differences and similarities. Geol. Soc. America Bull. *76*, p. 483–508.

Compagnoni, R. and B. Maffeo (1973): Jadeite-bearing metagranites l. s. and related rocks in the Mount Mucrone area (Sesia-Lanzo zone, western Italian Alps). Schweiz. mineral. petrogr. Mitt. *53*, p. 355–378.

Cortesogno, L., M. Galli, B. Messiga, G. M. Pedemonte e G. B. Piccardo (1975): Nota preliminare alla petrografia delle rocce eclogitiche del Gruppo di Voltri (Liguria Occidentale). Annali Museo Civ. St. Nat. Genova *80*, p. 325–343.

Cortesogno, L., W. G. Ernst, M. Galli, B. Messiga, G. M. Pedemonte and G. B. Piccardo (in press): Chemical petrology of eclogitic lenses in serpentinite, Gruppo di Voltri, Ligurian Alps. Jour. Geology.

Dal Piaz, G. V. (1974a): Le métamorphisme de haute pression et basse température dans l'évolution structurale du bassin ophiolitique alpino-apenninique I. Boll. Soc. Geol. Italy *93*, p. 1–31.

— (1974b): Le métamorphisme néo-alpin de haute pression et basse température dans l'évolution structurale du bassin ophiolitique alpino-apenninique. II. Schweiz. mineral. petrogr. Mi.. *54*, p. 399–424.

Dal Piaz, G. V., G. Gosso e G. Martinotti (1971): La II Zona Dioritico-Kinzigitica tra la Valsesia e la Valle d'Ayas (Alpi occidentali). Soc. Geol. Italiana Mem. *10*, p. 257–276.

Dal Piaz, G. V., J. C. Hunziker e G. Martinotti (1972): La zona Sesia–Lanzo e l'evoluzione tettonico-metamorfica delle Alpi nordoccidentali interne. Mem. Soc. Geol. Italy *11*, p. 433–460.

Dewey, J. F., W. C. Pitman, W. B. F. Ryan and J. Bonnin (1973): Plate tectonics and the evolution of the Alpine system. Geol. Soc. America Bull. *84*, p. 3137–3180.

Ernst, W. G. (1963): Petrogenesis of glaucophane schists. Jour. Petrology *4*, p. 1–30.

— (1971): Metamorphic zonations on presumably subducted lithospheric plates from Japan, California and the Alps. Contr. Mineral. Petrology *34*, p. 43–59.

— (1973): Interpretive synthesis of metamorphism in the Alps. Geol. Soc. America Bull. *84*, p. 2053–2078.

— (Ed.) (1975): Subduction zone metamorphism. Dowden, Hutchinson and Ross, Stroudsburg, PA, 445 p.

Ernst, W. G., Y. Seki, H. Onuki and M. C. Gilbert (1970): Comparative study of low-grade metamorphism in the California Coast Ranges and the Outer Metamorphic Belt of Japan. Geol. Soc. America Memoir *124*, 276 p.

Eskola, P. (1914): On the petrology of the Orijärvi Region in southwestern Finland. Bull. Comm. géol. Finland, No. 40, 279 p.

— (1921): On the eclogites of Norway. Vidensk.-selskapets Skr., Kristiania, I, Matematisk-Naturvidenskapelig Kl., No. 8, p. 1–118.

— (1939): Die metamorphen Gesteine, p. 263–407, in: T. F. W. Barth, C. W. Correns und P. Eskola: Die Entstehung der Gesteine. Springer-Verlag, Berlin, 407 p.

Essene, E. J., B. J. Hensen and D. H. Green (1970): Experimental study of amphibolite and eclogite stability. Phys. Earth Planet. Interiors *3*, p. 378–384.

Frey, M., J. C. Hunziker, W. Frank, J. Bocquet, G. V. Dal Piaz, E. Jäger and E. Niggli (1974): Alpine metamorphism of the Alps. Schweiz. mineral. petrogr. Mitt. *54*, p. 248–290.

Fry, N. and W. S. Fyfe (1971): On the significance of the eclogite facies in Alpine metamorphism. Verh. Geol. Bundesanst. Wien, Jahrg. 1971, p. 257–265.

Green, D. H. and A. E. Ringwood (1967): An experimental investigation of the gabbro to eclogite transformation and its petrological applications. Geochim. et Cosmochim. Acta *31*, p. 767–833.

Grover, J. E. and P. M. Orville (1969): The partitioning of cations between coexisting single- and multi-site phases with application to the assemblages orthopyroxene-clinopyroxene and orthopyroxene-olivine. Geochim. et Cosmochim. Acta *33*, p. 205–226.

Hey, M. H. (1954): A new revision of the chlorites. Mineral Mag. *30*, p. 277–292.

Hunziker, J. C. (1970): Polymetamorphism in the Monte Rosa, western Alps. Eclogae geol. Helv. *63*, p. 151–161.

— (1974): Rb-Sr and K-Ar age determination and the alpine tectonic history of the western Alps. Mem. Ist. Geol. Mineral., Univ. Padova, 31, 54 p.

Ito, K. and G. C. Kennedy (1971): An experimental study of the basalt-garnet granulite-eclogite transition. Geophys. Monograph Ser. *14*, p. 303–314.

Jäger, E., E. Niggli und E. Wenk (1967): Rb-Sr-Altersbestimmungen an Glimmern der Zentralalpen. Beiträge Geologiekarte Schweiz, Neue Folge, 134, 67 p.

Kitahara, S., S. Takenouchi and G. C. Kennedy (1971): Phase relations in the system MgO-SiO_2-H_2O at high temperatures and pressures. Am. Jour. Sci. *264*, p. 223–233.

Lambert, I. B. and P. J. Wyllie (1972): Melting of gabbro (quartz eclogite) with excess water to 35 kilobars, with geological applications. Jour. Geol. *80*, p. 693–708.

Laubscher, H. P. (1971a): Das Alpen-Dinariden-Problem und die Palinspastik der südlichen Tethys. Geol. Rundschau *60*, p. 813–833.

— (1971b): The large-scale kinematics of the western Alps and the northern Apennines and its palinspastic implications. Am. Jour. Sci. *271*, p. 193–226.

Lowrie, W. and W. Alvarez (1975): Paleomagnetic evidence for rotation of the Italian Peninsula. Jour. Geophysics, Res., *80*, p. 1579–1592.

MacGregor, I. D. and J. L. Carter (1970): The chemistry of clinopyroxenes and garnets of eclogite and peridotite xenoliths from the Roberts Victor Mine, South Africa. Phys. Earth Planet. Interiors *3*, p. 391–397.

Martini, J. (1972): Le métamorphisme dans les chaînes alpines externes et ses implications dans l'orogenèse. Schweiz. mineral. petrogr. Mitt. *52*, p. 257–275.

Matsui, Y. and S. Banno (1965): Intracrystalline exchange equilibria in silicate solid solutions. Proc. Japan Acad. *41*, p. 461–466.

Messiga, B. e G. B. Piccardo (1974): Rilevamento geo-petrografico e strutturale del Gruppo di Voltri. Il settore nord-orientale: la zona fra M. Tacco e M. Orditano. Mem. Soc. Geol. Italy, in press.

Miller, Ch. (1974): On the metamorphism of the eclogites and high-grade blueschists from the Penninic terrane of the Tauern window, Austria. Schweiz. mineral. petrogr. Mitt. *54*, p. 371–384.

Miyashiro, A. (1957): Chemistry, optics and genesis of the alkali amphiboles. Jour. Fac. Sci. Univ. Tokyo, sec. II, *11*, p. 57–83.

Mottana, A. and R. Bocchio (1975): Superferric eclogites of the Voltri group (Pennidic belt, Apennines). Contrib. Mineral. Petrology *49*, p. 201–210.

Mueller, R. F. (1962): Energetics of certain silicate solid solutions. Geochim. et Cosmochim. Acta *26*, p. 581–598.

— (1969): Kinetics and thermodynamics of intracrystalline distributions. Mineral. Soc. America, Special Paper No. 2, p. 83–94.

Niggli, E. (1960): Mineral-Zonen der alpinen Metamorphose in den Schweizer Alpen. XXI International Geol. Cong., Copenhagen, *13*, p. 132–138.

— (1970): Alpine Metamorphose und alpine Gebirgsbildung. Fortschr. Mineralogie *47*, p. 16–26.

— general coordinator (1973): Metamorphic map of the Alps: scale 1 : 1,000,000. UNESCO, Paris.

Niggli, E. und C. R. Niggli (1965): Karten der Verbreitung einiger Mineralien der alpidischen Metamorphose in den Schweizer Alpen (Stilpnomelan, Alkali-Amphibol, Chloritoid, Staurolith, Disthen, Sillimanit). Eclogae geol. Helv. *58*, p. 335–368.

Råheim, A. and D. H. Green (1974): Experimental determination of the temperature and pressure dependence of the Fe-Mg partition coefficient for coexisting garnet and clinopyroxene. Contr. Mineral. Petrology *48*, p. 179–203.

Ramberg, H. and G. W. deVore (1951): The distribution of Fe^{++} and Mg^{++} in coexisting olivines and pyroxenes. Jour. Geol. *59*, p. 193–210.

Ringwood, A. E. and D. H. Green (1966): An experimental investigation of the gabbro-eclogite transformation and some geophysical implications. Tectonophysics *3*, p. 383–427.

Saxena, S. K. (1973): Thermodynamics of rock-forming crystalline solutions. Springer-Verlag, New York, 188 p.

Scholle, P. A. (1970): The Sestri-Voltaggio Line: A transform fault induced tectonic boundary between the Alps and the Apennines. Am. Jour. Sci. *269*, p. 343–359.

Taylor, H. P. and R. G. Coleman (1968): O^{18}/O^{16} ratios of coexisting minerals in glaucophane-bearing metamorphic rocks. Geol. Soc. America Bull. *79*, p. 1727–1756.

Thompson, J. B., Jr. (1969): Chemical reactions in crystals. Am. Mineral. *54*, p. 341–375.

Van der Plas, L. (1959): Petrology of the northern Adula region, Switzerland (with particular reference to glaucophane-bearing rocks). Leidse Geol. Meded. *24*, p. 415–602.

Viterbo-Bassani, V. and C. Blackburn (1968): The eclogitic rocks of the "eclogitic micaschist formation", Sesia–Lanzo zone. Padova Univ., Ist. Geol. Mineral. Mem. *27*, 43 p.

Wenk, E. (1962): Plagioklas als Indexmineral in den Zentralalpen. Die Paragenese Calcit-Plagioklas. Schweiz. mineral. petrogr. Mitt. *42*, p. 139–152.

— (1970): Zur Regionalmetamorphose und Ultrametamorphose im Lepontin. Fortschr. Mineralogie *47*, p. 34–51.

Wenk, E. und F. Keller (1969): Isograde in Amphibolitserien der Zentralalpen. Schweiz. mineral. petrogr. Mitt. *49*, p. 157–198.

WETZEL, R. (1974): Hornblenden aus der Albit- bis Albitoligoklaszone zwischen Zermatt und Domodossola. Schweiz. mineral. petrogr. Mitt. *54*, p. 151–208.

YODER, H. S., Jr., and C. E. TILLEY (1962): Origin of basaltic magmas: an experimental study of natural and synthetic rock systems. Jour. Petrology *3*, p. 342–532.

ZIJDERVELD, J. D. A., G. J. A. HAZEN, M. NARDIN and R. VAN DER VOO (1970): Shear in the Tethys and the Permian paleomagnetism in the southern Alps, including new results. Tectonophysics *10*, p. 639–661.

Manuscript received June 3, 1976.